

---

# Balanced Conic Rectified Flow

---

**Shin seong Kim**  
 Yonsei University  
 t1tydl2@yonsei.ac.kr

**Mingi Kwon**  
 Yonsei University  
 kwonmingi@yonsei.ac.kr

**Jaeseok Jeong**  
 Yonsei University  
 jete\_jeong@yonsei.ac.kr

**Youngjung Uh\***  
 Yonsei University  
 yj.uh@yonsei.ac.kr

## Abstract

Rectified flow is a generative model that learns smooth transport mappings between two distributions through an ordinary differential equation (ODE). The model learns a straight ODE by reflow steps which iteratively update the supervisory flow. It allows for a relatively simple and efficient generation of high-quality images. However, rectified flow still faces several challenges. 1) The reflow process is slow because it requires a large number of generated pairs to model the target distribution. 2) It is well known that the use of suboptimal fake samples in reflow can lead to performance degradation of the learned flow model. This issue is further exacerbated by error accumulation across reflow steps and model collapse in denoising autoencoder models caused by self-consuming training. In this work, we go one step further and empirically demonstrate that the reflow process causes the learned model to drift away from the target distribution, which in turn leads to a growing discrepancy in reconstruction error between fake and real images. We reveal the drift problem and design a new reflow step, namely the *conic reflow*. It supervises the model by the inversions of real data points through the previously learned model and its interpolation with random initial points. Our conic reflow leads to multiple advantages. 1) It keeps the ODE paths toward real samples, evaluated by reconstruction. 2) We use only a small number of generated samples instead of large generated samples, 600K and 4M, respectively. 3) The learned model generates images with higher quality evaluated by FID, IS, and Recall. 4) The learned flow is more straight than others, evaluated by curvature. We achieve much lower FID in both one-step and full-step generation in CIFAR-10. The conic reflow generalizes to various datasets such as LSUN Bedroom and ImageNet. The project page is available at [https://grainsack.github.io/BC\\_rectified\\_flow\\_project\\_page/](https://grainsack.github.io/BC_rectified_flow_project_page/).

## 1 Introduction

Rectified flow [9, 28, 24, 25, 23] demonstrates state-of-the-art image generation with fewer sampling steps than diffusion models [6, 43, 37, 15, 41].  $k$ -rectified flow involves  $k$  reflow steps that make ODE paths smooth and straight [27]. This allows the model to generate high-quality images simply and efficiently in just one or a few steps. Intriguingly, *all rectified flow models* (Flux, SD3, and AuraFlow) achieve state-of-the-art quality with *1-rectified flow* and require about 30 NFEs (number of function evaluations) [9].

In this paper, we identify key limitations of  $k$ -rectified flow stemming from its reflow procedure, and propose to use real images and their inversions, combined with a Slerp-based perturbation loss, to

---

\*Corresponding author.

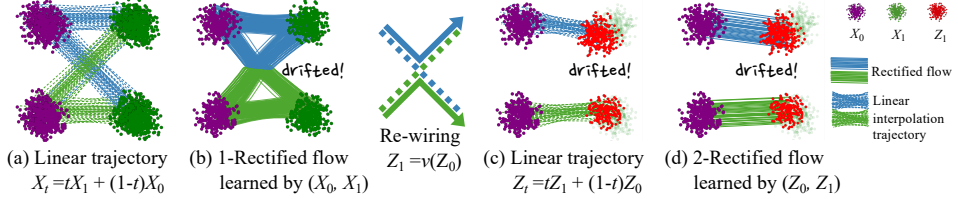


Figure 1: **Problem of rectified flow.** (a) By randomly pairing data  $X_0 \sim \pi_0$  and  $X_1 \sim \pi_1$ , linear interpolation trajectories are defined. (b) The 1-rectified flow connects  $X_0$  and  $X_1$  with a learned velocity field which is potentially inaccurate. After the 1-rectified flow, the trajectories are rewired to avoid crossing. (c) The trajectories for reflow are defined as linear interpolation trajectories between  $Z_0$  and the generated  $Z_1 = v(Z_0)$ . Note that  $Z_1$  is drifted away from  $\pi_1$ . (d) Consequently, the 2-rectified flow has a velocity field drifted away from  $X_1$ .

address them. Our core insight is that the degradation in performance cannot be fully explained by error accumulation or vanishing weight norms alone [18, 56]. Instead, we observe that the reflow process itself induces a drift away from the target distribution, leading to a measurable discrepancy between the model’s behavior on real and fake samples, which we later analyze through reconstruction error. 1) **The flow drifts away from the real distribution.** For example, in training a 2-rectified flow, random noise vectors and their generated images from the 1-rectified flow are reused as supervisory targets, which causes the ODE paths to diverge from real data. We empirically show that this results in a reconstruction performance gap between real and fake samples, and that Slerp-based supervision for real samples helps maintain alignment with the true distribution. 2) **The number of fake samples required for reflow is prohibitively large.** Our method leverages real samples and their conic neighbors to guide the flow with far fewer generated pairs, while maintaining competitive or superior performance. This efficiency makes the method scalable and less dependent on synthetic supervision. 3) **The reflow process degrades image quality in full-step generation.** By providing trajectory-level supervision rooted in real data geometry, our method enhances generation quality across 1-step, few-step, and full-step regimes, and mitigates the degradation in standard reflow training.

As a result, we successfully demonstrate better performance than existing  $k$ -rectified flow models. On CIFAR-10, we reduce the FID (Fréchet Inception Distance, [14]) of the existing 2-rectified flow from 12.21 to 5.98 while using only 7.2% of the generative pair, and show that the curvature of the ODE paths became straighter. We also introduce a new method for calculating curvature, which explains the time distribution sampling method. We provide various ablation studies and show that even with simple fine-tuning, the performance of existing  $k$ -rectified flow can be significantly improved.

## 2 Rectified Flow

Rectified flow [27] is a generative model that solves an ordinary differential equation (ODE) to induce a transition trajectory between two given data distributions  $\pi_0$  and  $\pi_1$ . Data  $X_0 \sim \pi_0$  and  $X_1 \sim \pi_1$  define linear trajectories  $X_t = (1 - t)X_0 + tX_1$  for  $t \in [0, 1]$ , as illustrated in Figure 1a. Then, a rectified flow  $v$  is an ODE on time  $t$  parameterized by  $\theta$ :

$$\frac{dZ_t}{dt} = v_\theta(Z_t, t) := \frac{1}{t}(Z_t - \mathbb{E}[(X_1 - X_0) | X_t = Z_t]) \quad (1)$$

We omit  $\theta$  for brevity. Liu et al. [27] propose a simplified mean squared error (MSE) loss for an ODE neural network to train velocity field  $v : \mathbb{R}^n \rightarrow \mathbb{R}^n$  as follows:

$$\arg \min_{\theta} \mathbb{E} \left[ \|X_1 - X_0 - v(tX_1 + (1 - t)X_0, t)\|^2 \right] \quad (2)$$

With  $t \sim \text{Uniform}([0, 1])$ . In image generation tasks,  $X_0 \sim \pi_0$  and  $X_1 \sim \pi_1$  are random noise and real images, sampled from a Gaussian distribution and the data distribution, respectively. Once the model has learned the velocity field, the rectified flow rewrites the trajectories in a non-crossing manner due to the inherent properties of ODEs, which enforce uniqueness and smoothness in trajectory evolution, preventing paths from intersecting in the continuous-time dynamics, as depicted in Figure 1b. It constitutes a 1-rectified flow model denoted by  $\mathbf{Z} = \text{RectFlow}((X_0, X_1))$ .

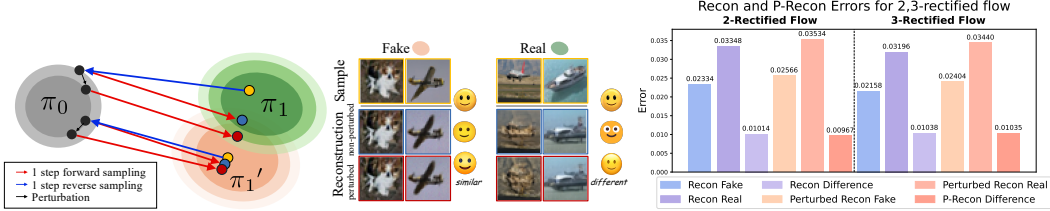


Figure 2: **(a) 2-rectified flow overfits fake samples.** Following the reverse and forward 2-rectified flow, fake images inherently return at similar images with or without perturbation at  $\pi_0$ . In contrast, real images return at different images and it is worse with perturbation, implying overfitting. **(b)** Reconstruction discrepancies emerge between real and fake images due to the use of fake-only pairs.

The  $k$ -rectified flow model learns a straighter sampling trajectory by repeating *reflow procedure*  $k$  times as follows. Following  $\mathbf{Z}^k$  from  $Z_0^k$  induces a generated pair  $(Z_0^k, Z_1^k)$  where  $(Z_0^0, Z_1^0) = (X_0, X_1)$ . It redefines the linear interpolation trajectory  $\mathbf{Z}_t^{k+1} = (1-t)Z_0^k + tZ_1^k$  for  $t \in [0, 1]$ , as shown in Figure 1c. Then, fine-tuning a velocity field  $v$  using Eq. (2) with  $(Z_0^k, Z_1^k)$  instead of  $(X_0, X_1)$  constitutes  $\mathbf{Z}^{k+1} = \text{RectFlow}((Z_0^k, Z_1^k))$ .

According to optimal transport theory, [45, 44, 10, 11] coupling the generated pairs  $(Z_0, v(Z_0))$  ensures that the interpolation trajectory preserves the marginal distributions of the original and target domains, as well as the linear interpolation trajectory between them [21, 2].  $k$ -rectified flow has superior quality of few-step sampling by straighter sampling trajectory, as shown in Figure 1d.

### 3 Improved Techniques for Reflow Step

In this section, we discuss the generated fake pairs in the original rectified flow and their problems. Then, we introduce real pairs and balanced-conic reflow which directly supervise the flow to reach the real data distribution. Finally, we provide detailed training configurations.

#### 3.1 Reflow steps drift the flow away from the real distribution.

As shown by Liu et al. [27], the trajectory  $Z_t^k$  between the generated pairs in the reflow process becomes smoother and straighter with each iteration of reflow, because the ODE induces a deterministic smooth solution while preserving the same marginal distribution as the original trajectory. This straightened path is essential for generating high-quality images with a small number of sampling steps rather than SDE-based generative models [15, 37, 35]. We use subscript  $F$  to denote the **fake** pairs from the original rectified flow as follows:

$$(Z_{0,F}^k, Z_{1,F}^k) := (Z_0^k, Z_1^k) \quad (3)$$

Where  $Z_0^k \sim \pi_0$  and  $Z_1^k = v(Z_0^k)$ .<sup>2</sup> To simplify notation and avoid confusion, we will denote the fake pair as  $(Z_{0,F}, Z_{1,F})$  when we do not need to consider the reflow step and, denote the  $k$ -th order of the rectified flow as  $(Z_{0,F}^k, Z_{1,F}^k)$ .

Beyond known issues such as error accumulation and model collapse [18, 56], we provide empirical evidence that reflow steps cause a distributional drift, observed through growing reconstruction discrepancies between real and fake samples. We provide empirical evidence of the accumulating drifts and suboptimality of the learned rectified flow. Figure 2a illustrates faithfulness and continuity<sup>3</sup> of a 2-rectified flow on both fake samples and real samples. As expected, fake images are mostly reconstructed by inversion and generation following the 2-rectified flow, i.e.,  $Z_1 \simeq v(v^{-1}(Z_1))$ . Also, an inversion of a fake sample and its perturbation land at similar images, i.e.,  $v(v^{-1}(Z_1)) \simeq v(v^{-1}(Z_1) + \varepsilon z)$  where we perturb it with  $\varepsilon = 0.05$ . In contrast, real images lose the main object by inversion and generation following the 2-rectified flow, i.e.,  $X_1 \neq v(v^{-1}(X_1))$ . Furthermore, real images are vulnerable to perturbation on their inversion, i.e.,  $v(v^{-1}(X_1)) \neq v(v^{-1}(X_1) + \varepsilon z)$ . To

<sup>2</sup>For brevity, we denote the forward generation process at the  $t$ -th sampling step as  $X_0 + \int_0^1 v_t(X_t, \cdot) dt := v(X_0)$  and backward process as  $X_1 + \int_0^1 v_t^{-1}(X_t, \cdot) dt := v^{-1}(X_1)$ , where  $v^{-1} = -v$ .

<sup>3</sup>We use the notion of continuity as in Lipschitz continuity: the generated images should be similar with the similar latents.

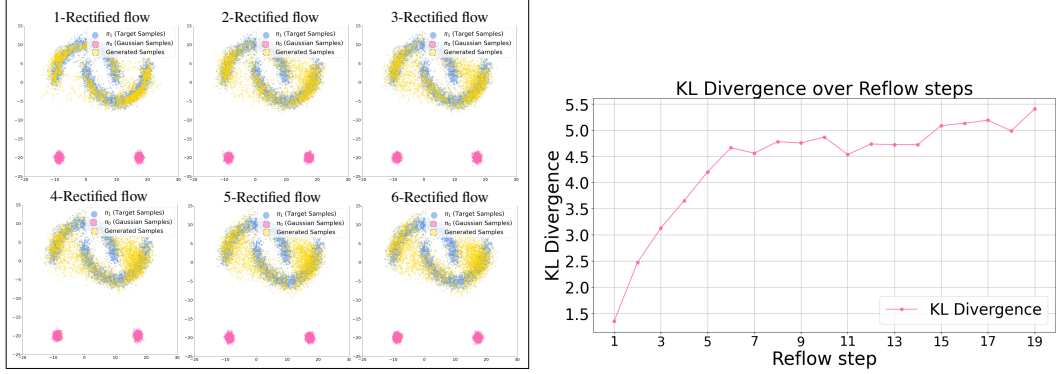


Figure 3: (a) As reflow steps increase, generated samples diverge from the target distribution. (b) This drift is further evidenced by the rising KL divergence from the real data distribution.

evaluate the faithfulness of a rectified flow to a dataset  $X$ , we measure the error between the sample and its reconstruction [4, 33] via the flow:

$$L_2^{\text{recon}}(X) = \mathbb{E}_{x \sim X} [\|x - v(v^{-1}(x))\|_2] \quad (4)$$

Instead of Lipschitz continuity, we practically evaluate the continuity of a rectified flow near samples from a dataset  $X$  by measuring a perturbed reconstruction error:

$$L_2^{\text{p-recon}}(X, \varepsilon) = \mathbb{E}_{x \sim X, z \sim \pi_0} \|x - v(v^{-1}(x) + \varepsilon z)\|_2, \quad (5)$$

where  $\varepsilon$  is the strength of perturbation. The lower perturbed reconstruction error near the real samples  $L_2^{\text{p-recon}}(X_1)$  indicates the more continuous generative model near the real samples.<sup>4</sup> Figure 2b compares  $L_2^{\text{recon}}$  of real and fake samples, and  $L_2^{\text{p-recon}}$  near real and fake samples.  $L_2^{\text{recon}}$  is higher at the real samples than the fake samples. It indicates that the 2,3-rectified flow drifts away from the real samples. Furthermore,  $L_2^{\text{p-recon}}$  is lower near the fake samples than the real samples. It indicates that the 2-rectified flow suffers from crossing between real samples.

Critically, the original reflow accumulates the drift over recursive reflow steps. This drift is an innate phenomenon because the supervision from a shifted distribution does not steer the flow toward the real distribution. Figure 3a provides empirical evidence of the accumulating drift in a toy two moons dataset [32]. The successive reflow steps cause the fake (yellow) data to diverge further from the real (blue) target distribution. Furthermore, Figure 3b illustrates the progressive increase in KL divergence between the fake distribution and the target distribution, providing clear evidence of this phenomenon.<sup>5</sup> We provide a solution to mitigate this issue in Section 3.3 and 3.4.

### 3.2 Real pair

The previous subsection has unveiled the pitfall of supervision using fake pairs: samples from the domain distribution, e.g., Gaussian, and their codomain following a rectified flow. Instead of the fake pairs, we propose to use the real samples and their inverse following a reverse rectified flow, defined by :

$$\text{Real pair}(Z_{0,R}, X_1) := (v^{-1}(X_1), X_1) \quad (6)$$

with  $X_1 \sim \pi_1$  where  $v$  is the 1-rectified flow and we abuse the term *real pair* although the  $Z_{0,R}$  is not real. As in the original rectified flow, where it was optionally provided, it is safe and easy to use reverse rectified flow without stochasticity because it inherently produces a deterministic solution, and using real images does not contradict the original purpose because the noise  $v^{-1}(X_1)$  is generated using  $v^{-1}$ . To avoid confusion, from now on, we will refer to  $(X_0, v(X_0))$  as a *fake pair* (generated pair), where  $v(X_0)$  is a fake (generated) image, and  $(v^{-1}(X_1), X_1)$  as a *real pair*, where  $X_1$  is a real image.

<sup>4</sup>We measure the reconstruction and perturbed reconstruction error with 1-step Euler sampling.

<sup>5</sup>The KL divergence is measured between Gaussian mixture approximations of the fake and real samples.

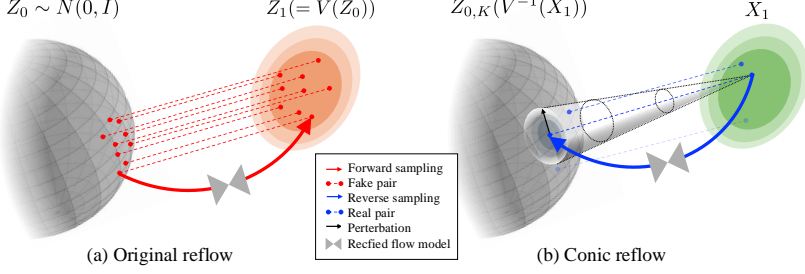


Figure 4: **Illustration of original fake pairs and our real pairs.** (a) The original rectified flow supervises 2-rectified flow with fake pairs ( $Z_0, v_\theta(Z_0)$ ). (b) Our conic reflow supervises 2-rectified flow with real pairs ( $v_\theta^{-1}(X_1), X_1$ ) and their conic neighbors.

### 3.3 Conic reflow

Building upon the basic pairing of real samples with their reverse noises, we introduce conic reflow, which expands their influence on the domain distribution to their neighboring areas, as shown in Figure 4b. When we train the model, we use spherical linear interpolation (Slerp) between the reverse noise  $Z_{0,R}$  and a randomly sampled noise  $\epsilon \sim \mathcal{N}(0, I)$  with the interpolation ratio  $\zeta$ :

$$\text{Slerp}(Z_{0,R}, \epsilon, \zeta) = \frac{\sin((1 - \zeta)\phi)}{\sin(\phi)} Z_{0,R} + \frac{\sin(\zeta\phi)}{\sin(\phi)} \epsilon, \quad (7)$$

where  $\phi = \arccos(Z_{0,R} \cdot \epsilon)$  denotes the angle between  $Z_{0,R}$  and  $\epsilon$ . Then we define a conic inverse from a real sample  $X_1$ :

$$\text{Conic}(X_1, \epsilon, \zeta, t) = tX_1 + (1 - t)\text{slerp}(Z_{0,R}, \epsilon, \zeta), \quad (8)$$

where  $Z_{0,R} = v_\theta^{-1}(X_1)$ , and  $t \in [0, 1]$ . During training, we sample  $\epsilon$  and  $\zeta$  multiple times to let the target flow stochastically cover the nearby domain. As the collection of the paths over multiple iterations looks like a cone, we name our method as *conic reflow*. The schedule of interpolation weight  $\zeta$  is deferred to Section 3.5. Our training objective with conic reflow is:

$$\hat{\theta} = \arg \min_{\theta} \int_0^1 \mathbb{E} \left[ w_t \left\| X_1 - \text{slerp}(Z_{0,R}, \epsilon, \zeta) - v_\theta(\text{Conic}(X_1, \epsilon, \zeta, t)) \right\|^2 \right] dt \quad (9)$$

Where  $t \sim \exp([0, 1])$ ,  $\zeta \sim \text{slerp schedule}([0, 1])$ ,  $\epsilon \sim \mathcal{N}(0, I)$ , and  $w_t$  is weighting function (default=1). Slerp is commonly used for interpolation in the noise space of generative models, as it preserves vector magnitudes on the Gaussian hypersphere and enables smooth semantic transitions [47, 16]. In our case, Slerp serves as a geometry-aware regularizer that improves the alignment between numerically inverted real samples and the underlying data manifold. Rather than simply reusing generated samples, we supervise the model using real samples and their perturbed inversions to reduce reconstruction loss discrepancies observed during reflow. This approach not only mitigates distributional drift but is also aligned with adversarial robustness strategies studied in inverse problems and reconstruction-based neural networks [3, 1]. From this perspective conic reflow provides localized supervision that encourages stability and continuity around real data points in the noise space.

### 3.4 Balanced conic rectified flow

We design a new reflow procedure which consists of our conic reflow and the original reflow. For each training iteration, we design different training schemes for real pairs and fake pairs. We alternate between conic reflow steps with real pairs ( $Z_{0,R}, X_1$ ) and original reflow steps with fake pairs. It encourages the trajectories to head toward the exact real distribution while fake pairs ensure the entire domain distribution to receive supervision. Fake Pairs: For fake pairs, we proceed with the reflow process exactly as it was done in the original rectified flow model. Its training objective  $\hat{\theta}$  as follows:

$$\arg \min_{\theta} \mathbb{E} \left[ \|Z_{1,F} - Z_{0,F} - v_\theta(tZ_{1,F} + (1 - t)Z_{0,F})\|^2 \right], \quad (10)$$

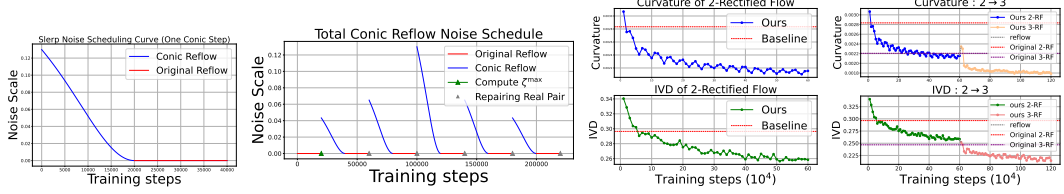


Figure 5: (a) Slerp noise schedule for single conic reflow and (b) Total slerp schedule. (c) Curvature and IVD during training, and (d) From 2- to 3-rectified flow.

with  $t \sim \exp([0, 1])$ . The entire training objective of our method is as follows for the given fake pair  $(Z_{0,F}, Z_{1,F})$  and real pair  $(Z_{0,R}, X_1)$ :

$$\min_v \int_0^1 \left[ \left\| \chi_{\text{fake}} \cdot \left( \dot{Z}_{t,F} - v_\theta(Z_{t,F}) \right) + \chi_{\text{real}} \cdot \left( X_1 - \text{slerp}(Z_{0,R}, \epsilon, \zeta) - v_\theta(\text{Conic}(X_1, \epsilon, \zeta, t)) \right) \right\|^2 \right] dt \quad (11)$$

where  $\chi_{\text{fake}}$  and  $\chi_{\text{real}}$  are indicator functions for given index subsets  $U_{\text{real}}$  and  $U_{\text{fake}}$  such that  $U_{\text{real}} \cup U_{\text{fake}} = \mathbb{N}$ . Then, for  $i \in \mathbb{N}$ :

$$\chi_{\text{fake}} = \begin{cases} 1 & \text{if } i \in U_{\text{fake}} \\ 0 & \text{else} \end{cases}, \quad \chi_{\text{real}} = \begin{cases} 1 & \text{if } i \in U_{\text{real}} \\ 0 & \text{else.} \end{cases} \quad (12)$$

The notation  $\zeta$ ,  $\text{Conic}(\cdot)$ ,  $\epsilon$ , and  $w_t$  follows the definitions in Section 3.3.

### 3.5 Detailed training schemes

In this section, we provide a more detailed explanation of our proposed training schemes, including visualizations of the Slerp scheduling and maximum Slerp noise magnitude. The maximum magnitude of the Slerp noise,  $\zeta^{\max} \in (0, 0.5]$  is selected in accordance with our intuition that it is the point where the discrepancy between the perturbed reconstruction errors of real and fake samples is maximized. After a warm-up phase of training steps, we compute  $\zeta^{\max}$  using 10,000 images each from the real and fake. The value is selected based on the following hyperparameter  $\zeta^{\max}$ :

$$\zeta^{\max} := \max_{\zeta \in (0, 0.5]} \mathbb{E}_{\substack{x \sim X_1 \\ z \sim Z_{1,F}}} [\|v_\theta(\text{Slerp}(z_{0,R}, \epsilon, \zeta)) - x\|_2 - \|v_\theta(\text{Slerp}(z_{0,F}, \epsilon, \zeta)) - z\|_2] \quad (13)$$

where  $\epsilon \sim \mathcal{N}(0, I)$ , with  $z_{0,R} = v_\theta^{-1}(x)$  and  $z_{0,F} = v_\theta^{-1}(z_{1,F})$  denoting the inverse noise estimates for the real and fake samples, respectively. Figure 5(a) shows a single conic reflow noise schedule in training steps (For CIFAR-10 and ImageNet, we set  $\zeta^{\max}$  to 0.13 and 0.23, respectively). Each conic is trained to progressively reduce the noise scale over time. Specifically, the Slerp noise schedule  $\zeta(t')$  is defined as  $\zeta(t') := \zeta^{\max} \cdot \frac{2t'^2}{1+t'^2}$ ,  $t' \in [0, 1]$ , where  $t' = 1$  corresponds to the start of training and  $t' = 0$  to the end. This design follows the intuition from traditional diffusion models [15], where noise is progressively reduced to guide samples toward realism. To strengthen the real image trajectory during training, we periodically update the real sample pairs used in the reflow process. Figure 5(b) illustrates an example of conic reflow with updated real pairs, assuming 220K total training steps for visualization. When the number of updates is 2K, we schedule the maximum noise magnitude  $\zeta^{\max}$  by scaling it according to the pattern  $[K, K-1, \dots, 1, 2, \dots, K]$ , assigning  $\zeta^{\max}/K$  to the smallest value and  $\zeta^{\max}$  to the midpoint. The noise increases linearly in the first half and decreases symmetrically in the second half. The full pseudocode for our training method is provided in Appendix K.

## 4 Experiments

We conducted experiments to evaluate the effectiveness of our method. Our findings demonstrate: Superiority over original reflow in terms of (1) Quality of the results, (2) Straightness of the flow, (3) Mitigation of distribution shift, as well as (4) Ablation study, (5) Generalization to other datasets.

Method	NFE ( $\downarrow$ )	IS ( $\uparrow$ )	FID ( $\downarrow$ )
<b>One-Step Generation (Euler solver, N=1)</b>			
1-Rectified Flow	1	1.13 (9.08)	378 (6.18)
<b>2-Rectified Flow</b>			
Original (+Distill)	1	8.08 (9.01)	12.21 (4.85)
Ours (+Distill)	1	<b>8.79 (9.11)</b>	<b>5.98 (4.16)</b>
RF++ <sup>†</sup> [24]	1	8.87	4.43
RF++ <sup>†</sup> (+ours)	1	8.87	<b>4.22</b>
<b>3-Rectified Flow</b>			
Original (+Distill)	1	8.47 (8.79)	8.15 (5.21)
Ours (+Distill)	1	<b>8.84 (8.96)</b>	<b>5.48 (4.68)</b>
<b>Full Simulation (Runge–Kutta (RK45), Adaptive N)</b>			
1-Rectified Flow	127	<b>9.60</b>	<b>2.58</b>
<b>2-Rectified Flow</b>			
Original	110	9.24	3.36
Ours	104	<b>9.30</b>	<b>3.24</b>
<b>3-Rectified Flow</b>			
Original	104	9.01	3.96
Ours	98	<b>9.14</b>	<b>3.70</b>

Table 1: One-step and full-simulation comparison of 2,3 Rectified Flows on CIFAR-10.

**Experimental setup** Most of our experiments are conducted on CIFAR-10 [20]. The IVD, curvature, reconstruction, and perturbed ( $0.05\epsilon$ , 1-step) reconstruction error values reported were computed using 10,000 random samples, with the expectation taken over these samples. We employ Scipy’s RK45[46], a 5(4) Runge-Kutta method with adaptive step size and step count determined by specified tolerances, following the same parameters [37]. Further details on the training configurations are provided in Appendix J.

#### 4.1 Image quality

Our method achieves better FID and IS scores across all sampling steps, i.e., 1-step, few-step, and full-step generations, as shown in Table 1 and Figure 6. Notably, we use only 300K fake pairs, significantly fewer than the 4M fake pairs used in the original rectified flow, demonstrating the efficiency of our approach. Furthermore, our method outperforms the original in generation quality with RK sampling, even with a lower NFE. We also apply our method to Rectified++ [24] and compare generation quality. While RF++<sup>†</sup> uses 800K synthetic pairs, our variant uses 600K fake pairs and 50K real images, achieving better FID. This indicates that our method generalizes well to reflow-based generative models. Detailed settings for RF++<sup>†</sup> are provided in Appendix J.

Additionally, our method produces images with superior quality even when applying the same distillation in the original rectified flow [27] as compared to solid (ours) and dashed (original) lines, and star (ours) and rectangle (original) in Figure 6. These results suggest that our method produces a more favorable initial velocity field than the original rectified flow. A detailed comparison of precision and recall scores is provided in Appendix B. Furthermore, we show in Appendix D that fine-tuning the original rectified flow using only real images and their reverse noise pairs effectively reduces reconstruction discrepancy and quickly improves generation quality. Additional performance comparisons on more complex datasets and higher-resolution images are presented in Sections 4.5 and 4.6. To further contextualize the performance of reflow-based methods, we also report the unconditional generation quality of pretrained diffusion models on CIFAR-10 in Appendix N.

#### 4.2 Straightness

We evaluate trajectory straightness using curvature, following prior works [27, 23]. Straighter trajectories reduce discretization error under few step solvers, improving sample quality [39, 5]. For any continuously differentiable process  $\mathbf{Z} = \{Z_t\}$ , the curvature is measured by :

$$S(\mathbf{Z}) = \int_0^1 \mathbb{E} \left[ \left\| (Z_1 - Z_0) - \dot{Z}_t \right\|^2 \right] dt \quad (14)$$

Additionally, it is known that  $S(\mathbf{Z}) = 0$  indicates exact straightness.

**Relationship between curvature and initial velocity delta (IVD)** While curvature captures trajectory straightness, it does not fully explain 1-step sampling quality, which depends solely on the initial velocity. We propose Initial Velocity Delta (IVD) to directly evaluate the accuracy of the

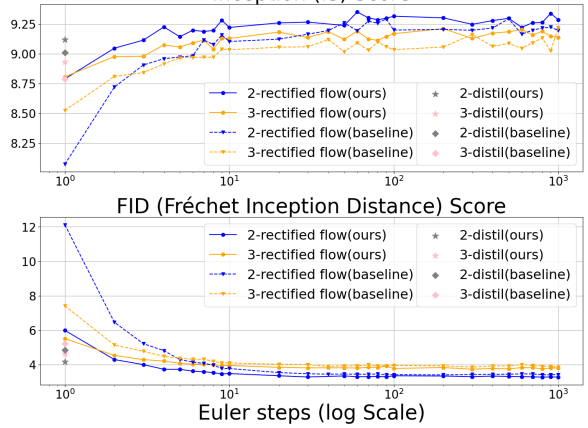


Figure 6: CIFAR-10 generation quality across Euler steps.

initial velocity and its impact on 1-step generation. The calculation method for IVD is provided in the equation below:

$$IVD(\mathbf{Z}, t_0) = \mathbb{E} \left[ \left\| (Z_1 - Z_0) - \dot{Z}_{t_0} \right\|^2 \right] \quad (15)$$

**Curvature and initial velocity delta.** Our approach demonstrates improved trajectory straightening and better preservation of the initial velocity direction. As shown in Figure 5(c), our method consistently achieves lower curvature and IVD values than the original, indicating a more stable trajectory even with fewer fake pairs. Furthermore, Figure 5(d) highlights that applying an additional reflow step from 2-rectified to 3-rectified flow further reduces both curvature and IVD, reinforcing the effectiveness of our training method.

### 4.3 Reconstruction with perturbation to address drift from the real distribution

We empirically show that incorporating real data pairs via Slerp-based supervision in the reflow step significantly improves the preservation of real image trajectories. As illustrated in Figure 7(a), the original rectified flow exhibits a clear reconstruction error gap between real and fake images, whereas our method progressively narrows this gap during training. Figure 7(b) highlights two key aspects. First, in terms of reconstruction error, our method better preserves real trajectories and mitigates overfitting to fake samples. Second, the lower perturbed reconstruction error suggests that the model more accurately aligns the velocity field around real images, leading to improved robustness against perturbations.

### 4.4 Ablation study

We report results from an ablation study on various settings of our proposed framework, comparing four configurations: (1) without Slerp noise; (2) reflow using just a single real pair; (3) our full method; and (4) the original 2-rectified flow. The comparison focuses on 1-step generation quality, curvature, IVD(Initial Velocity Delta), reconstruction error, and perturbed reconstruction error.

#### 4.4.1 Benefits of incorporating real data via slerp-based perturbation training

Model	FID	IS	Curvature	IVD	Recon Real	Recon Fake	Perturbed Real	Perturbed Fake
Original	12.21	8.08	0.002837	0.295078	0.033668	0.024106	0.035481	0.026270
<b>Ours* (Slerp + conic)</b>	<b>5.98</b>	<b>8.79</b>	<b>0.002295</b>	0.253334	<b>0.019404</b>	0.023139	<b>0.022382</b>	0.025206
Fixed Real Pair	6.69	8.59	0.002313	0.242444	0.020227	0.020607	0.022890	0.022914
No Slerp	6.60	8.57	0.002322	<b>0.240884</b>	0.023380	<b>0.020154</b>	0.026063	<b>0.022496</b>

Table 2: An ablation table comparing various 2-rectified models across multiple metrics: FID, IS (1-step), Curvature, IVD, and errors (Recon Real/Fake, Perturbed Real/Fake).

**Benefits of adding noise via Slerp** Adding noise via Slerp avoids trajectory crossover, preserving a straighter path relative to real images. This leads to improved trajectory quality and enhances 1-step sampling efficiency. Moreover, using Slerp results in lower reconstruction error for real images compared to not using it. This demonstrates that Slerp-based noise perturbation helps stably maintain the trajectory and local neighborhood structure of reverse noise corresponding to real images. In particular, it plays a key role in reducing the reconstruction discrepancy we observe between real and fake samples during reflow, thereby effectively mitigating the distributional drift that occurs in later iterations.

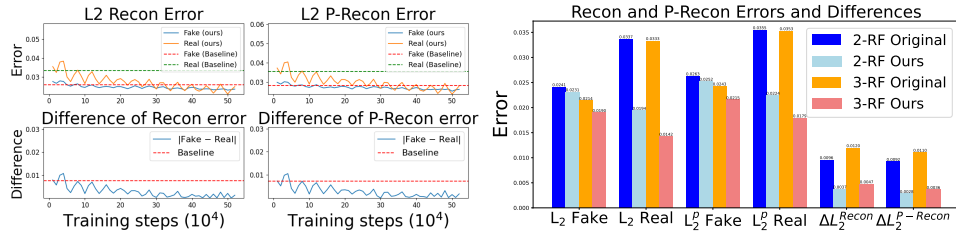


Figure 7: Reconstruction and perturbed reconstruction error across training iterations.

**Effect of real pair injection and refreshing** Incorporating real pairs into training improves trajectory fidelity and 1-step generation quality by anchoring learning closer to the target distribution. Notably, fixing the real pair only once leads to inferior performance, while periodically refreshing reverse noise achieves better FID, IS, and lower reconstruction errors. This highlights the importance of continuously updating real-sample guidance throughout training to maintain alignment with real data trajectories.

Additional experiments, including  $k = 4$  generation quality, precision/recall, low fake pair settings, and real-only supervision, are provided in Appendices C and E.

#### 4.4.2 Slerp noise patterns and lerp

In this section, we show that our Slerp-based reflow method consistently improves 1-step generation quality, even when the Slerp noise pattern varies. To support this claim, we train 2-rectified flow models using different Slerp schedules, including patterns where the noise gradually increases, gradually decreases, or first increases and then decreases. We also include a baseline where Slerp is replaced with Lerp for comparison. All experiments are conducted with a batch size of 256, and training is performed for 300K iterations. Each setting uses 300K fake pairs and 60K real pairs for training on Cifar 10. Other configurations remain identical to those described in Section 4 and Appendix J.

Category	Method	Schedule Type	IS ( $\uparrow$ )	FID ( $\downarrow$ )
Slerp	Ours	$\zeta_k^{\max} : \zeta^{\max} / K \rightarrow \zeta^{\max} \rightarrow \zeta^{\max} / K$	<b>8.72</b>	<b>6.63</b>
	Strictly Increasing	$\zeta_k^{\max} : \zeta^{\max} / K \rightarrow \zeta^{\max}$	8.48	<u>6.64</u>
	Strictly Decreasing	$\zeta_k^{\max} : \zeta^{\max} \rightarrow \zeta^{\max} / K$	8.45	6.70
Lerp	Linear Interpolation	$(1-\zeta) \cdot v^{-1}(X_1) + \zeta \cdot \epsilon, \zeta \in [0, \zeta^{\max}]$	8.46	7.50

Table 3: Each method uses Slerp or Lerp-based noise trajectories. The best and second-best values are bolded and underlined, respectively.

As shown in Table 3, we observe three key findings. First, Slerp-based schedules consistently outperform Lerp in both FID and IS, suggesting that Slerp more effectively preserves the reverse noise trajectories of real images. Second, the strictly increasing noise schedule yields better performance than the decreasing one, indicating that progressive noise injection improves training stability. Third, our method achieves the highest IS while maintaining comparable FID to the best baseline, demonstrating improved sample diversity without compromising generation quality.

#### 4.5 More complex dataset (Unconditional generation on ImageNet 64×64)

On ImageNet 64×64 [7], our method consistently improves unconditional generation quality over the original model. Using the same setup as CIFAR-10, we train a 1-rectified flow for 700K steps with batch size 256. The original uses **1M** fake pairs, while our method uses **600K** fake and 60K real pairs. As shown in Table 4, Although 60K real images may be insufficient to fully cover the target distribution of ImageNet compared to CIFAR-10, our method still yields substantial gains in FID and Recall. This suggests that even limited real data can provide strong guidance in mitigating distributional drift. Moreover, it improves reconstruction error, perturbed reconstruction error, recall, and precision (see Table 5 and Appendix F), demonstrating its ability to reduce distributional drift even on large-scale datasets.

#### 4.6 High-resolution image generation

In this section, we assess the generalizability of our method on the LSUN Bedroom dataset [52] at a resolution of 256×256. We use the same hyperparameters, time schedule, and EMA settings as in the experiments by Liu et al. [27]. We use 60K fake pairs and 5K real pairs, while the original uses 120K fake pairs. Despite GPU limitations on the larger LSUN dataset, our method consistently outperformed the original in image quality. Figure 8 shows superior few step generation quality, and with adaptive step sampling (RK45), our approach achieved comparable quality with significantly fewer fake pairs than the original. Further details on the training configurations are provided in Appendix J. For comparisons under different random seeds, refer to Appendix I.

Metric	FID		IS	
	RK-45	Euler	RK-45	Euler
1-rectified flow	23.1	369.8	12	1.1
2-rectified flow	31.2	39.7	10.8	<b>10.4</b>
<b>Ours</b>	<b>28.2</b>	<b>37.8</b>	<b>11.4</b>	10.3

Table 4: FID and IS across rectified flows using RK-45 and Euler solver on ImageNet.



Figure 8: Visual and quantitative comparison on LSUN. **Left:** 2-row layout showing original (**top**) and ours (**bottom**) for each solver (1-step, 2-step, RK). **Right:** evaluation metrics.

## 5 Related work

Recent efforts to improve rectified flow models focus on modifying the time distribution, loss functions, or model architectures [24, 18]. Some works incorporate real data pairs or introduce discriminator-based regularization to reduce the effect of out-of-distribution samples [18]. Others analyze model degradation through the lens of denoising autoencoders, attributing performance drop to the vanishing of weight norms caused by repeated training on synthetic pairs [56]. PerFlow takes a different approach by constructing piecewise linear intermediate paths to stabilize reflow training [50]. In contrast to these works, our method introduces a perturbation-based supervision using real data inversions.

## 6 Conclusion and future work

We propose balanced conic reflow, a simple yet effective method that addresses key limitations of traditional rectified flow by incorporating real pairs through a Slerp-based perturbation strategy. Our approach improves generation quality across multiple settings, while requiring significantly fewer synthetic samples. Its plug-and-play nature makes it compatible with various flow-based generative models, such as InstaFlow and SD3 [28, 9]. Future directions include extending our method with additional loss functions or integrating it with diffusion-based synthetic supervision [24, 18]. Moreover, our strategy may complement recent frameworks such as Rectified Diffusion [48], which demonstrate that reflow-like improvements are possible even without retraining  $v$ -prediction-based flow matching models, where conic reflow can further help preserve real image trajectories and reduce reconstruction discrepancy without relying on linear interpolation paths or discriminator-based supervision.

## Acknowledgment

This work was partly supported by the National Research Foundation of Korea (RS-2023-00223062) and an IITP grant (RS-2020-II201361, RS-2024-00439762) funded by the Korean government (MSIT).

# Balanced Conic Rectified Flow

## Supplementary Material

### A Detailed settings

**CPU and GPU settings** All experiments were conducted on a machine with an Intel Core i9-10980XE CPU (18 cores, 3.00GHz) and four NVIDIA GeForce RTX 3090 GPUs (24GB VRAM each). The system was equipped with 128GB of DDR4 RAM.

**Using exponential distribution of timesteps for training** The trajectory crossovers during the reflow process are more frequent near the noise or image endpoints (i.e., when closer to  $X_0$  or  $X_1$ ) [24]. To focus the training more effectively on these regions with high crossover frequency, we employed an exponential distribution. This phenomenon can be clearly observed in A1a, where we computed the top-k indices of the predicted velocity during the sampling process. The curvature is significantly higher near the start and end indices, indicating more crossovers at those points. Based on this observation, we adopted an exponential distribution<sup>6</sup> rather than a uniform distribution, as illustrated in A1b.

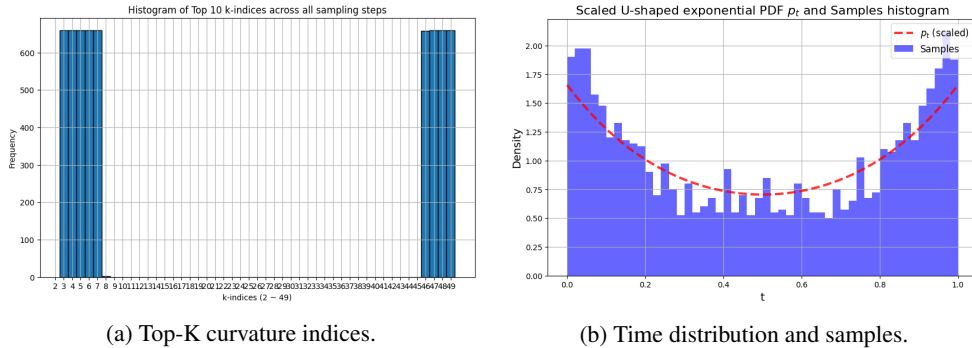


Figure A1: Top-K (K=10) curvature indices and U-shape exponential time distribution with sampled data. For visualization convenience, the U-shaped probability density function  $p_t$  was scaled so that the area under the curve equals 1.

**$U_{\text{fake}}$  and  $U_{\text{real}}$**  The training schedule for conic reflow and original reflow is split into two phases. In the first half, conic and original reflows alternate to prevent bias toward either real or fake pairs. In the second half, only the original reflow is used to address the data imbalance, as fake pairs are far more abundant than real pairs. For instance, if total training step is  $N = 100$ , then  $U_{\text{real}} = \{1, 3, 5, 7, \dots, 49\}$  and  $U_{\text{fake}} = \{2, 4, 6, 8, \dots, 50, 51, 52, \dots, 100\}$ .

### B Recall and Precision

In this section, we evaluate the performance of our method compared to the original rectified flow using recall and precision metrics. These metrics allow us to analyze how well the generated data covers the real data distribution (recall) and how accurate the generated samples are compared to the real data (precision) [22].

We conduct the evaluation on the CIFAR-10 dataset, which consists of 60,000 real images combined with 50,000 synthetic images. For sampling, we utilize Euler sampling to ensure consistency across experiments.

As shown in A1, the results highlight key differences between multi-step and 1-step sampling:

<sup>6</sup>More explicitly, we use  $p_t(u) \propto \exp(au) + \exp(-au)$  on  $u \in [0, 1]$  with  $a = 3$

- **Multi-step sampling:** Both our method and the original exhibit similar precision and recall values, indicating comparable performance in this setting.
- **1-step sampling:** Precision shows only a slight difference of approximately 0.85% on average, suggesting that both methods perform nearly identically in terms of precision. However, recall reveals a more significant advantage for our method:
  - On average, our method achieves 4.5% higher recall across all settings.
  - Specifically, for 2-Rectified Flow, our method outperforms the original by 5.5% in recall.

These findings indicate that while the precision of our method is nearly identical to the original, its higher recall demonstrates superior coverage of the real data distribution. Therefore, we can interpret these results as evidence that our method produces a more comprehensive and balanced representation of the underlying data distribution compared to the original.

Method	NFE	Precision ( $\uparrow$ )	Recall ( $\uparrow$ )
<b>2-Rectified Flow</b>			
<i>Full Step Generation</i>			
Ours	104	0.691	<b>0.605</b> (+0.005)
Original	104	<b>0.696</b> (+0.005)	0.600
<i>One step Generation</i>			
Ours	1	0.687	<b>0.583</b> (+0.055)
Original	1	<b>0.695</b> (+0.008)	0.528
<b>3-Rectified Flow</b>			
<i>Full Step Generation</i>			
Ours	104	0.691	<b>0.599</b> (+0.007)
Original	104	<b>0.698</b> (+0.007)	0.592
<i>One step Generation</i>			
Ours	1	0.682	<b>0.592</b> (+0.03)
Original	1	<b>0.691</b> (+0.009)	0.562

Table A1: Comparison of 2- and 3-Rectified Flows under different NFE settings, highlighting the better results in bold.

## C Extreme number of reflow process ( $k = 4$ )

In this section, we compare the generative quality, curvature, IVD of our method and the original under a setting with an extreme number of reflow processes ( $k = 4$ ), which is higher than the typical settings of  $k = 2$  or  $k = 3$ .

Method	NFE	IS ( $\uparrow$ )	FID ( $\downarrow$ )	Precision ( $\uparrow$ )	Recall ( $\uparrow$ )
<b>4-Rectified Flow</b>					
Ours	100	<b>9.076</b>	<b>4.195</b>	0.696	<b>0.585</b>
Original	100	8.951	4.490	<b>0.705</b>	0.584
Ours	1	<b>8.808</b>	<b>5.662</b>	<b>0.690</b>	<b>0.581</b>
Original	1	8.597	6.580	0.688	0.576

Table A2: Comparison of IS, FID, precision, and recall for 4-Rectified Flow between Ours and Original. The better values are highlighted in bold.

Method	Curvature ( $\downarrow$ )	IVD ( $\downarrow$ )
<b>4-Rectified Flow</b>		
Ours	<b>0.00176</b>	<b>0.20787</b>
Original	0.00186	0.21812

Table A3: Comparison of curvature and IVD for 4-Rectified Flow between Ours and Original rectified flow. The better values are highlighted in bold.

As shown in Table A2 and A3:

- **1-Step generation quality:** Our method outperforms the original in both FID and IS, demonstrating superior generative performance.
- **Multi-step generation quality:** Similarly, our method shows better results compared to the original.

- **Additional metrics:** Our method achieves better curvature and IVD compared to the original. This indicates that our method forms a velocity field that enables the solution trajectory to be straighter during the reflow process and better preserves the direction of the initial velocity, ensuring it aligns more closely with the overall trajectory.

These findings show that our method preserves the distribution of real images while preventing bias toward fake images. Even with  $k > 3$ , our method improves the reflow process and makes it robust for extreme reflow step settings.

## D Fine-tuning with real pairs improves a pre-trained rectified flow model

We demonstrate the effect of fine-tuning a pretrained rectified flow model using only 60,000 real pairs. For this experiment, we used the official rectified flow CIFAR-10 checkpoints available on GitHub.<sup>7</sup> With minimal additional training, we observe a noticeable improvement in 1-step quality as shown in Figure A2(a). Additionally, both curvature and IVD values decrease rapidly as illustrated in Figure A2(b). These results show that applying our method to a 2- or 3-rectified flow model, previously trained with standard techniques, effectively improves 1-step generation quality even with a small number of real pairs. Figure A2(b) also shows fine-tuned version has lower curvature and IVD than the original, indicating that our method is straighter than the original. Furthermore, the fine-tuned version has lower recon and p-recon differences between real and fake images, indicating that our method reduces the bias toward fake samples. For visualization convenience, IVD was scaled by  $10^{-2}$ .

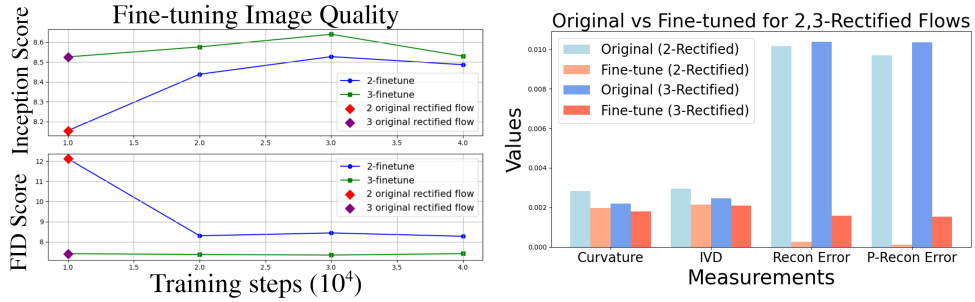


Figure A2: (a) Comparison of image quality between the original rectified model and our fine-tuned model across training steps (left). (b) Comparison of measurements for original and fine-tuned models for 2- and 3-rectified flows (right).

## E Using even fewer fake samples and reflow just real pair

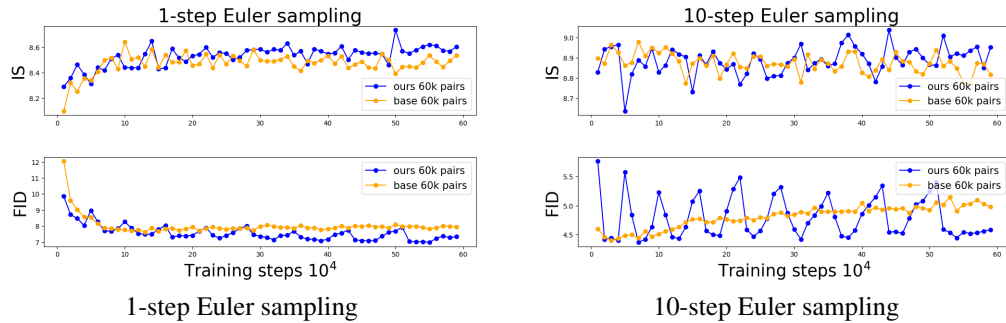


Figure A3: FID and IS score for original and ours 2-rectified flow (using 60k fake pairs)

**Extreme case (60k fake pair(original) and + 60k fake pair Real pair(ours))** Figure A3 compares the generation quality of the 2-rectified flow trained with an extremely small number of fake pairs.

<sup>7</sup>Checkpoints are available at: <https://github.com/gnobitab/RectifiedFlow>.

As shown in the figure, when the number of fake pairs is very limited, the 1-step image generation quality shows slight improvement. However, reflow training under such limited data coverage tends to overfit to the narrow fake distribution, which leads to a decline in generation quality over multiple steps, despite the gains observed in 1-step performance.

In contrast, our approach preserves the path for real images during the conic reflow step, even with an extremely small number of fake pairs (60k). This results in not only improved 1-step quality but also mitigates the degradation in multi-step generation quality compared to the original.

**Reflow just using real pair** We also conduct experiments under the extreme setting where reflow is trained using only real image pairs, excluding any synthetic samples. While this setup leads to slight improvements in 1-step generation quality, we observe progressive degradation in full-step performance as training continues. This limitation arises from the fact that real pairs offer accurate supervision only in the local neighborhood of the data manifold. Without the diversity and coverage provided by synthetic samples, the model struggles to generalize its velocity field across the entire generation trajectory.

To validate this observation, we compare the following three settings: (1) Real only (no Slerp), (2) Real only with Slerp-based supervision, and (3) Our full method combining real and fake pairs with Slerp. As shown in Table A4, setting (2) improves over (1), but both underperform compared to our full method:

Setting	1-step (IS / FID)	RK-step (IS / FID)
(1) Real only (no Slerp)	8.21 / 6.93	8.65 / 5.13
(2) Real only (+ Slerp)	8.53 / 6.71	9.02 / 4.47
(3) Ours (real + fake + Slerp)	<b>8.79 / 4.16</b>	<b>9.30 / 3.24</b>

Table A4: Performance comparison using only real pairs, real pairs with Slerp supervision, and our full method.

These results show that while Slerp-based perturbed supervision enhances the effectiveness of real image, the combination of real and synthetic samples achieves better 1-step and multi-step generation quality.

## F Generalization to complex dataset: Imagenet 64×64

In this section, we evaluate how well our method generalizes on the ImageNet 64×64 dataset. We compare our method with the original by using 1) reconstruction and perturbed reconstruction errors, and 2) their difference. The evaluation shows that our approach is not only limited to smaller datasets like CIFAR-10 but also extends effectively to more challenging datasets. All precision and recall values are computed using 100k real images and 50k synthetic images. Reconstruction and perturbed reconstruction errors are obtained using a 2-step Euler solver, where reverse noise is perturbed with Slerp by  $\epsilon = 0.1$ . Both reconstruction and perturbed reconstruction errors are computed over a total of 12k images.

As shown in Table A5, our method significantly reduces reconstruction errors for both real and fake images compared to the original. This includes perturbed cases, where the gap between real and fake reconstruction errors (Difference and Difference Perturbed) is notably smaller in our approach. These results demonstrate that our method effectively mitigates the increasing discrepancy between real and fake images during the reflow process. For qualitative results on reconstruction and perturbed reconstruction images for both fake and real images, please refer to Figure A4 and A5.

	Fake Recon	Real Recon	Perturbed Fake Recon	Perturbed Real Recon	Difference	Difference Perturbed
Ours (Euler 2-step)	<b>0.01727</b>	<b>0.02138</b>	<b>0.02735</b>	<b>0.03076</b>	<b>0.00410</b>	<b>0.00340</b>
Original (Euler 2-step)	0.02566	0.03273	0.03665	0.04261	0.00707	0.00596

Table A5: Comparison of Reconstruction errors and differences between Original and Ours on ImageNet 64x64 using the Euler 2-step solver.

## G RF++ $^\dagger$ and RF++ $^\dagger$ (+Ours) extended training results (500K steps)

In this section, we report extended training results beyond 300K iterations to demonstrate that our method continues to outperform the original RF++ $^\dagger$ .

As shown in Table A6, RF++ $^\dagger$ (+Ours) achieves better FID and IS scores compared to RF++ $^\dagger$ . This suggests that our Slerp-based perturbation method leads to more efficient reflow training, effectively preserving straight paths to real image distributions. All experiments use the same training configurations as described in Appendix J.

Model	Steps	IS ( $\uparrow$ )	FID ( $\downarrow$ )	Solver
RF++ $^\dagger$ (+Ours)	1-step	<b>9.15</b>	<b>3.84</b>	Heun 2nd
RF++ $^\dagger$	1-step	9.04	4.14	Heun 2nd
RF++ $^\dagger$ (+Ours)	2-step	<b>9.36</b>	<b>3.03</b>	Heun 2nd
RF++ $^\dagger$	2-step	9.24	3.16	Heun 2nd

Table A6: Extended training results (500K steps) for RF++ $^\dagger$  and RF++ $^\dagger$ (+Ours).

## H Qualitative results of reconstruction and perturbed reconstruction

Figure A12, A13, A14 provide a qualitative comparison of reconstruction between the original and ours. Figure A15 provide a qualitative comparison of the perturbed reconstruction between the original and ours (Cifar 10). As shown in the figures, the rectified flow model trained with our reflow procedure preserves the structure of real objects more effectively, whereas the original generates images that deviate significantly from the original object after undergoing reconstruction or perturbed reconstruction.

## I Qualitative comparison on Lsun dataset

We provide additional qualitative results in Figure A6,A7, A8, A9, A10, A11 demonstrating that our method achieves better generation quality than the original under few-step sampling settings.

## J Misc. configurations

Our experiments on CIFAR10 are configured as follows. For rectified flow, we utilize the same network architecture as the rectified flow model based on DDPM++ in [37, 27] with batch size 256. The training process is smoothed using an exponential moving average (EMA) with a decay rate of 0.999999, following the approach in Song et al. [37]. The Adam optimizer [8] is used with a learning rate of 2e-4 and a dropout rate of 0.15 is applied.

We train RF++ $^\dagger$  following the configuration (F) from Lee et al. [24], which includes EDM initialization, an exponential time distribution, and LPIPS-Huber-1/t loss, with a batch size of 128. For training, we use 800K fake pairs for RF++ and 600K fake pairs with an additional 50K real pairs for RF++ $^\dagger$ (+ours). Both models are optimized using Adam with an EMA decay of 0.9999. We generate 50,000 synthetic images to compute FID using the official RF++ implementation, which employs Heun’s second-order solver [24]. For evaluation, we report results using the best checkpoint selected during 300K training iterations. The best FID and IS score obtained with 500K iterations (see Appendix G) is also based on the same configuration, and evaluated using the official RF++ and guided-diffusion [A3] implementation without modification.

For the high-resolution (LSUN), both our method and the original 2-rectified flow were trained for 600,000 steps with a batch size of 16. Training started from the same 1-rectified flow checkpoints from the official rectified flow repository. During inference, all models used fixed seeds and identical noise conditions corresponding to the sampling steps.

## K Pseudocode

---

**Algorithm 1:** Full Algorithm (Red text indicates our addition)

---

**Input:** Coupling  $(X_0, X_1)$  of  $\pi_0$  and  $\pi_1$ ; velocity model  $v_\theta : \mathbb{R}^d \rightarrow \mathbb{R}^d$   
**Output:**  $v_{\hat{\theta}_{\text{conic}}}$

```

1 Training:
2  $\hat{\theta} = \arg \min_\theta \mathbb{E} [\|X_1 - X_0 - v_\theta(tX_1 + (1-t)X_0, t)\|^2]$ , where  $t \sim \text{Uniform}([0, 1])$ 
3 Sampling:
4 Draw forward flow:  $dZ_{t,F} = v_{\hat{\theta}}(Z_{t,F}, t) dt$ , starting from  $Z_{0,F} \sim \pi_0$ 
5 Draw backward flow:  $(Z_{0,R}, X_1)$  following  $dZ_{t,R} = v_{\hat{\theta}}^{-1}(Z_{t,R}, t) dt$ , with  $X_1 \sim \pi_1$ 
6 Balanced Conic Reflow:
7 Initialize : Total training step =  $\mathbb{N}$ , Repairing step =  $\mathcal{T}$ ,  $cnt = 0$ ,  $\chi_{\text{fake}}$ ,  $\chi_{\text{real}}$ 
8 for  $t \in (0, \mathbb{N})$  do
9   if  $t == t_{\zeta^{\max}}$  then
10    | Compute  $\zeta^{\max}$  using Eqn. 13
11   if  $cnt == \mathcal{T}$  then
12    | Generate new real pair:  $(Z_{0,R}, X_1) \leftarrow (v_{\theta_{\text{conic}}}^{-1}(X_1), X_1)$ 
13    |  $\zeta_k^{\max} \leftarrow \zeta^{\max}/k$ 
14    |  $cnt \leftarrow 0$ 
15   else
16    | Train: Update  $\hat{\theta}_{\text{conic}}$ 
17    |  $\arg \min_\theta \mathbb{E} [\|\chi_{\text{fake}} \cdot (\dot{Z}_{t,F} - v_\theta(Z_{t,F})) + \chi_{\text{real}} \cdot (X_1 - \text{slerp}(Z_{0,R}, \epsilon, \zeta) - v_\theta(\text{Conic}(X_1, \epsilon, \zeta, t)))\|^2]$ 
18   |  $cnt += 1$ 
19 (Optional) Distillation: Learn neural network  $\hat{T}$  to distill the  $k$ -rectified flow, so that  $Z_{1,F}^k \approx \hat{T}(Z_{0,F}^k)$ 

```

---

## L Limitation

While our method demonstrates strong improvements in reflow process, one limitation remains in the choice of the maximum Slerp noise magnitude  $\zeta^{\max}$ , which is dependent on the training dataset. We select  $\zeta^{\max}$  by measuring reconstruction discrepancy between real and fake samples after a warm-up phase, and choosing the noise scale that maximizes this gap. While this aligns well with our problem formulation and intuition, providing a theoretically explicit solution remains challenging due to the unknown intrinsic dimension of the training dataset. It may be beneficial to incorporate additional factors into the decision process. For example, from the perspective of information theory, the ratio between real and fake pairs may serve as a guideline by comparing their information content (e.g., entropy), and the intrinsic dimension of the data manifold may also provide useful signals for determining an appropriate noise scale [A1, A2].

## M Implementation details

**Slerp.** Below is the Python implementation of our spherical linear interpolation (Slerp), used to interpolate between the reverse noise  $Z_{0,R}$  and a randomly sampled noise  $\epsilon \sim \mathcal{N}(0, I)$  with ratio  $\zeta$ :

```
def slerp_ours(t, v0, v1, DOT_THRESHOLD=0.9995):
    c = True
    if not isinstance(v0, np.ndarray):
        c = True
        v0 = v0.detach().cpu().numpy()
    if not isinstance(v1, np.ndarray):
        c = True
        v1 = v1.detach().cpu().numpy()

    v0_copy = np.copy(v0)
    v1_copy = np.copy(v1)

    v0 = v0 / np.linalg.norm(v0)
    v1 = v1 / np.linalg.norm(v1)
    dot = np.sum(v0 * v1)

    if np.abs(dot) > DOT_THRESHOLD:
        print("do lerf")
        return torch.lerp(t, v0_copy, v1_copy)

    theta_0 = np.arccos(dot)
    sin_theta_0 = np.sin(theta_0)
    theta_t = theta_0 * t
    sin_theta_t = np.sin(theta_t)

    s0 = np.sin(theta_0 - theta_t) / sin_theta_0
    s1 = sin_theta_t / sin_theta_0
    v2 = s0 * v0_copy + s1 * v1_copy

    return torch.from_numpy(v2).to("cuda") if c else v2
```

**Noise scheduler.** We define the nonlinear Slerp noise schedule as:

```
def noise_scheduler(max_steps, max_noise):
    schedule = []
    for step in range(max_steps):
        t = step / max_steps
        noise = max_noise * 2 * (1 - 1 / (1 + t**2))
        schedule.append(noise)
    return schedule
```

**Scheduled reflow during training.** During training, conic reflow is periodically triggered and the noise schedule is dynamically adjusted:

```
if i_effective == warmup_steps:
    max_noise = compute_zeta_max(0.01, 0.5)
    # Equation (8): starting noise magnitude = 0.01, end = 0.5
    (...)

if i_effective % 100000 == 0:
    add_noise = True
    c_n = 0
    patail_max_noise = max_noise / noise_decay
    noise_decay += decay_direction
    # Start decay_direction is -1
    if noise_decay == 1:
        decay_direction = 1
    elif noise_decay == k:
```

```

decay_direction = -1
alpha = noise_scheduler(max_steps + 5, patail_max_noise)

```

**Applying conic reflow.** At scheduled noise injection steps, we replace  $z$  using Slerp between the original  $z$  and Gaussian noise:

```

if conic_rf:
    if add_noise:
        x, z, c, _ = next(train_iter_conic)
        noise_batch = torch.randn_like(z).to(device) * (1 - 1e-5)
        z = slerp_ours(alpha[-1 - c_n], z, noise_batch)
        if cnt % gradient_accumulation_steps == 0:
            print('conic reflow(slerp):', alpha[-1 - c_n], 'noise_step:', c_n)
            add_noise = False
    (...)

# Sample t, zt
t = sample_t(exponential_distribution, x.shape[0], arg.a).to(device)
zt = (1 - t).view(-1, 1, 1, 1) * x + t.view(-1, 1, 1, 1) * z
target = z - x

# Forward pass
pred = model(zt, t, c)
# Predicted x
pred_x = zt - pred * t.view(-1, 1, 1, 1)

```



## N Unconditional generation model quality

Method	NFE ( $\downarrow$ )	IS ( $\uparrow$ )	FID ( $\downarrow$ )
<b>Full Simulation (Euler Solver, N=2000)</b>			
VP SDE [37]	2000	9.58	2.55
sub-VP SDE [37]	2000	9.56	2.61
NCSN++ (VE SDE) [37]	2000	9.83	2.31
DDPM [15]	1000	9.46	3.21
<b>Adaptive Step Simulation (Runge–Kutta (RK45), Adaptive N)</b>			
VP ODE [37]	140	9.37	3.93
sub-VP ODE [37]	146	<b>9.46</b>	3.16
NCSN++ (VE ODE) [37]	176	<b>9.35</b>	5.38
LSGM [42]	147	-	<b>2.10</b>
PFGM [49]	110	<b>9.68</b>	<b>2.35</b>
EDM [17]	35	<b>9.84</b>	<b>2.04</b>
1-Rectified Flow	127	<b>9.60</b>	<b>2.58</b>
2-Rectified Flow	110	9.24	3.36
<b>2-Rectified Flow Ours</b>	104	9.30	3.24
3-Rectified Flow	104	9.01	3.96
<b>3-Rectified Flow Ours</b>	98	9.14	3.70
FM-OT [26]	142	-	6.35
OT-CFM [40]	100	-	4.44
Simple ReFlow [18]	9	-	<b>2.23</b>
<b>One-Step Simulation (Euler Solver, N=1)</b>			
VP ODE (+Distill) [37]	1	1.20 (8.73)	451 (16.23)
sub-VP ODE (+Distill) [37]	1	1.21 (8.80)	451 (14.32)
NCSN++ (VE ODE) (+Distill) [37]	1	1.18 (2.57)	461 (254)
1-Rectified Flow (+Distill)	1	1.13 (9.08)	378 (6.18)
2-Rectified Flow (+Distill)	1	8.08 (9.01)	12.21 (4.85)
2-Rectified Flow++ <sup>†</sup> [24]	1	9.03	4.14
2-Rectified Flow++ <sup>†</sup> (+Ours)	1	<b>9.15</b>	3.84
<b>2-Rectified Flow Ours (+Distill)</b>	1	8.79 (9.11)	5.98 (4.16)
3-Rectified Flow (+Distill)	1	8.47 (8.79)	8.15 (5.21)
<b>3-Rectified Flow Ours (+Distill)</b>	1	8.84 (8.96)	5.48 (4.68)
<b>Diffusion + Distillation</b>			
DDIM Distillation [30]	1	8.36	9.36
DMD [51]	1	-	3.77
Diff-Instruct [31]	1	<b>9.89</b>	4.53
PD [34]	1	8.69	8.34
DFNO [53]	1	-	4.15
SlimFlow (EDM teacher) [57]	1	-	4.53
SlimFlow (1-Rectified flow teacher)	1	-	5.81
SID, ( $\alpha = 1.2$ ) [55]	1	<b>9.98</b>	<b>1.92</b>
<b>Consistency Model</b>			
CD [38]	1	<b>9.48</b>	3.55
CT [38]	1	8.49	8.70
ICT [36]	1	<b>9.54</b>	<b>2.83</b>
ECT [12]	1	-	3.60
sCT [29]	1	-	<b>2.97</b>
IMM [54]	1	-	3.40
MeanFlow [13]	1	-	<b>2.92</b>
CTM [19]	1	-	5.19
CTM + GAN [19]	1	-	<b>1.98</b>

Table A7: Unconditional generation quality with various diffusion-based models on CIFAR-10. **Blue** rows highlight the top-5 baselines for 1-NFE, and **red** rows for Adaptive NFE (RK-45). The lowest FID and highest IS scores in each setting are **bolded**.



(a) Real Image



(b) Reconstruction Image (Ours)



(c) Perturbed Recon Image (Ours)



(d) Real Image



(e) Reconstruction Image (Base)



(f) Perturbed Recon Image (Base)

Figure A4: Qualitative comparison of **real** image reconstruction and perturbed reconstruction results between the baseline and our method using the 2-rectified flow trained on the ImageNet dataset. The **bottom** row presents the original method, while the **top** row presents our method.



(a) Fake Image



(b) Reconstruction Image (Ours)



(c) Perturbed Recon Image (Ours)



(d) Fake Image



(e) Reconstruction Image (Base)



(f) Perturbed Recon Image (Base)

Figure A5: Qualitative comparison of **fake** image reconstruction and perturbed reconstruction results between the original and our method using the 2-rectified flow trained on the ImageNet dataset. The **bottom** row presents the original method, while the **top** row presents our method.

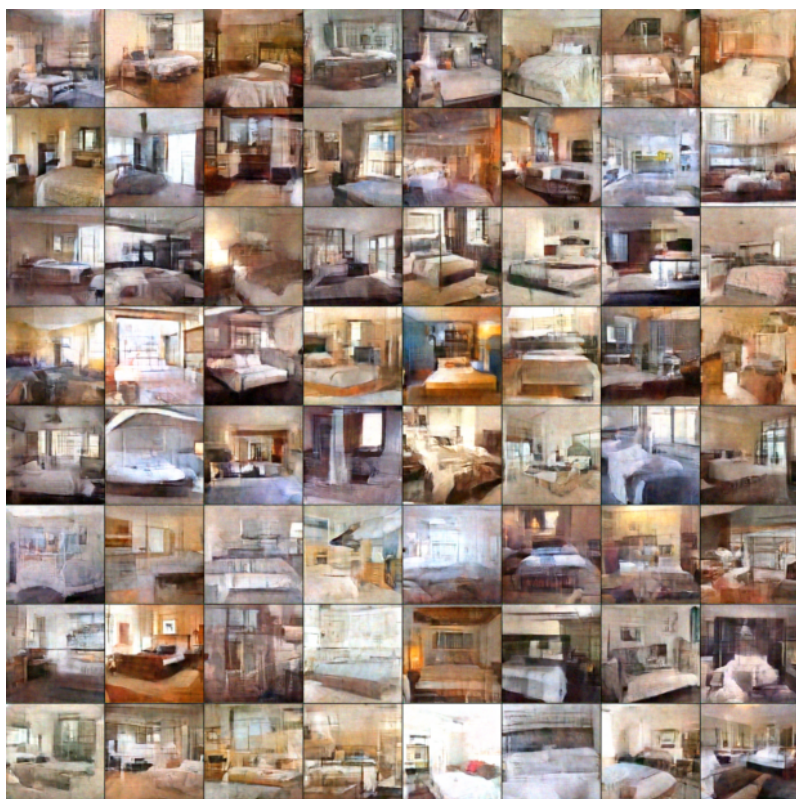
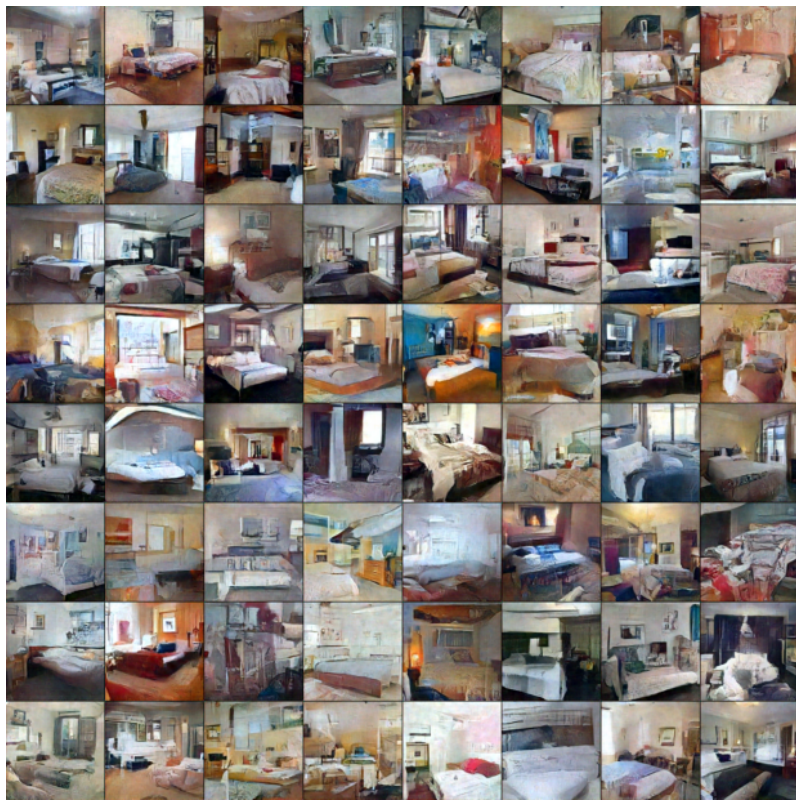


Figure A6: Ours (**up**) and Original (**down**) 2-rectified flow (1-step, seed 1)

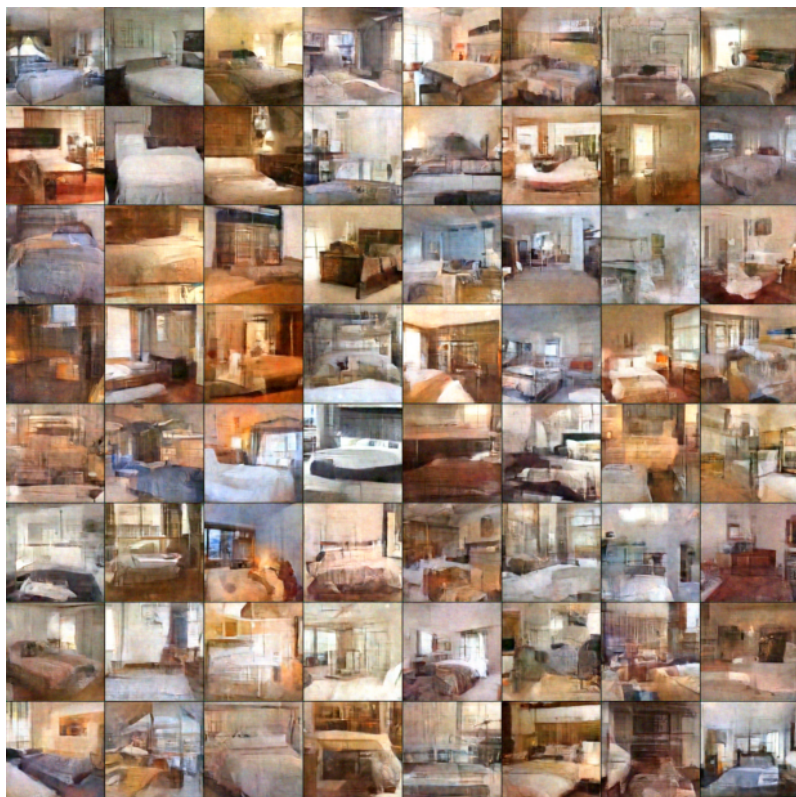


Figure A7: Ours (**up**) and Original (**down**) 2-rectified flow (1-step, seed 2)

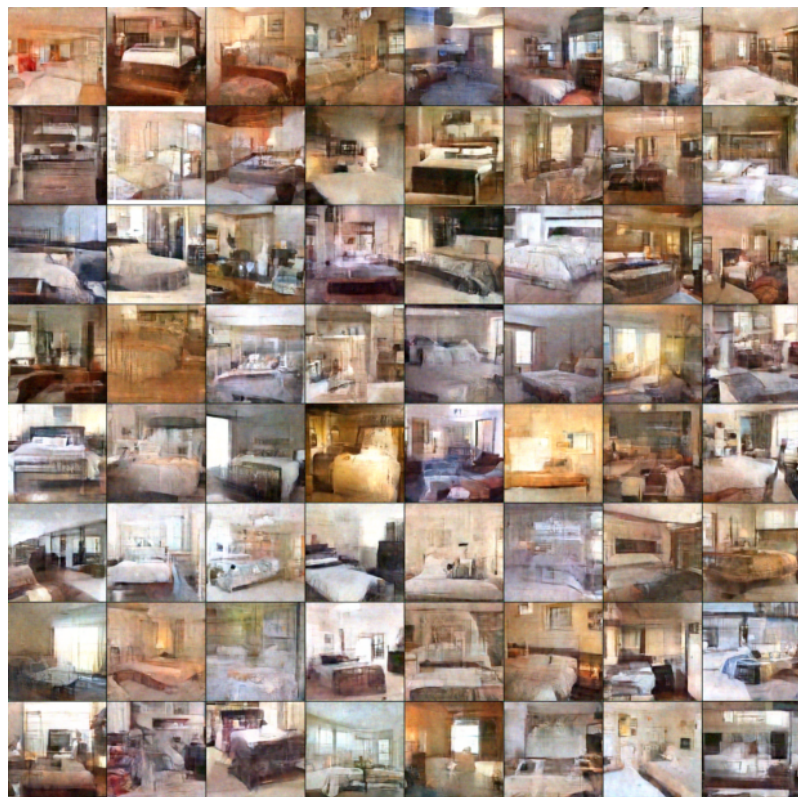


Figure A8: Ours (**up**) and Original (**down**) 2-rectified flow (1-step, seed 3)

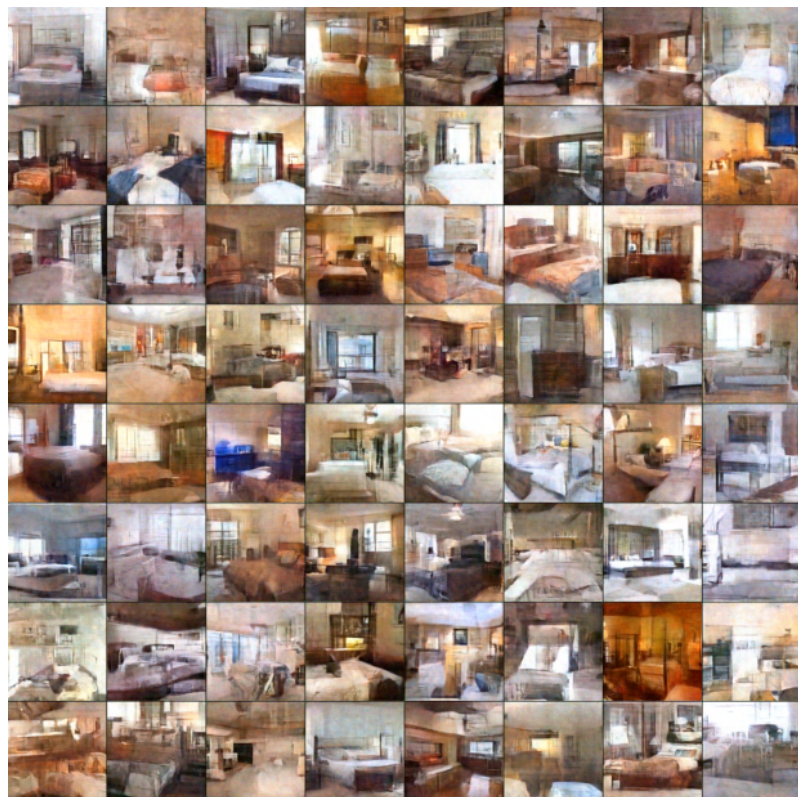


Figure A9: Ours (**up**) and Original (**down**) 2-rectified flow (1-step, seed 333)

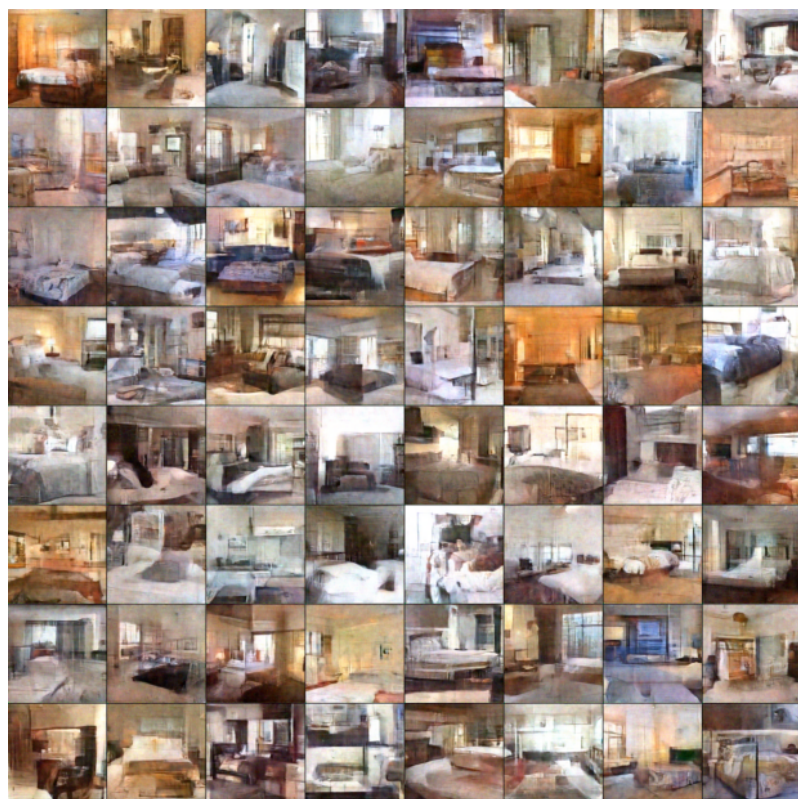


Figure A10: Ours (**up**) and Original (**down**) 2-rectified flow (1-step, seed 555)

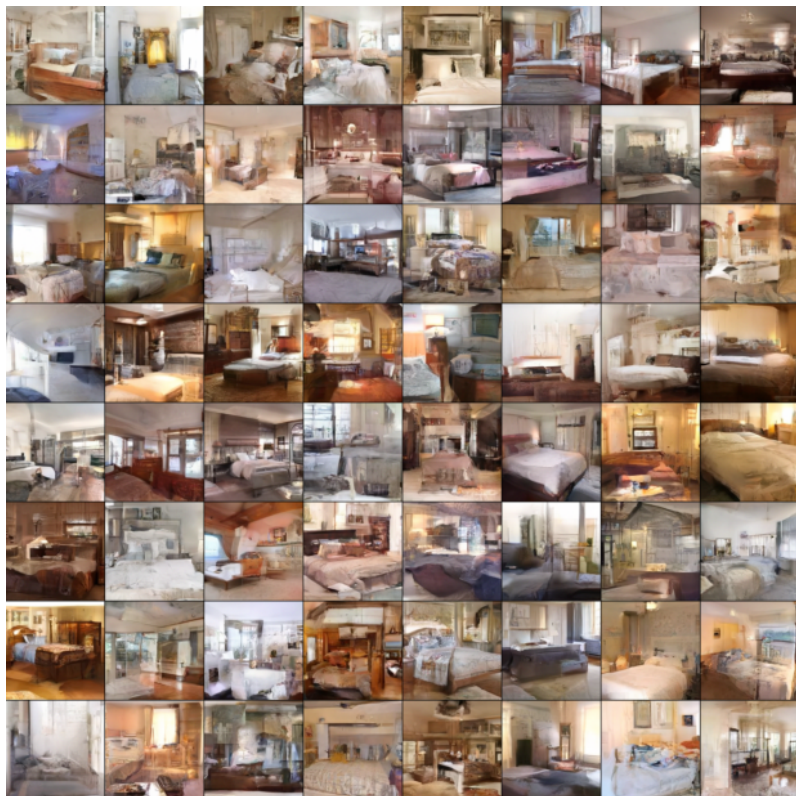


Figure A11: Ours (**up**) and Original (**down**) 2-rectified flow (2-step, seed 785)

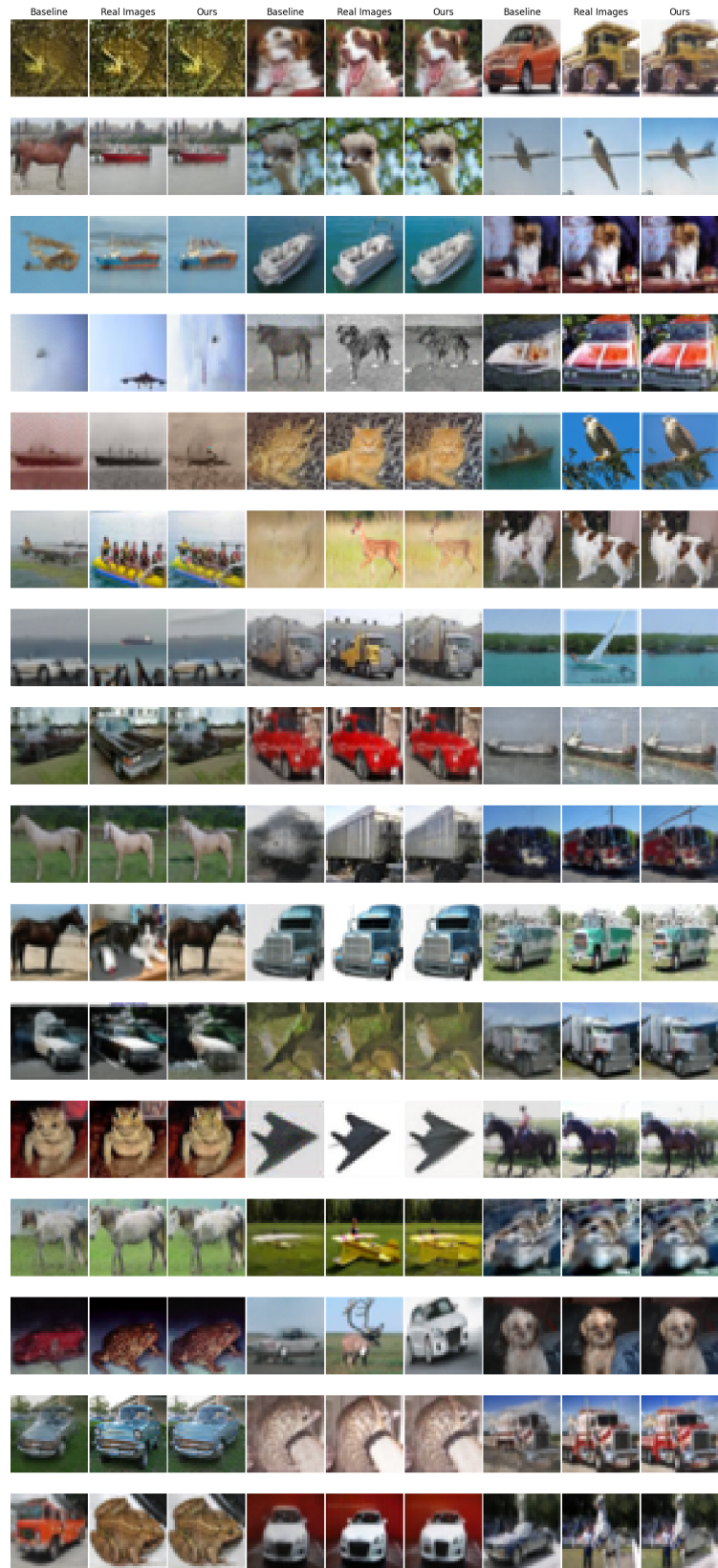


Figure A12: Compare with reconstruction image to original (1-step Euler)

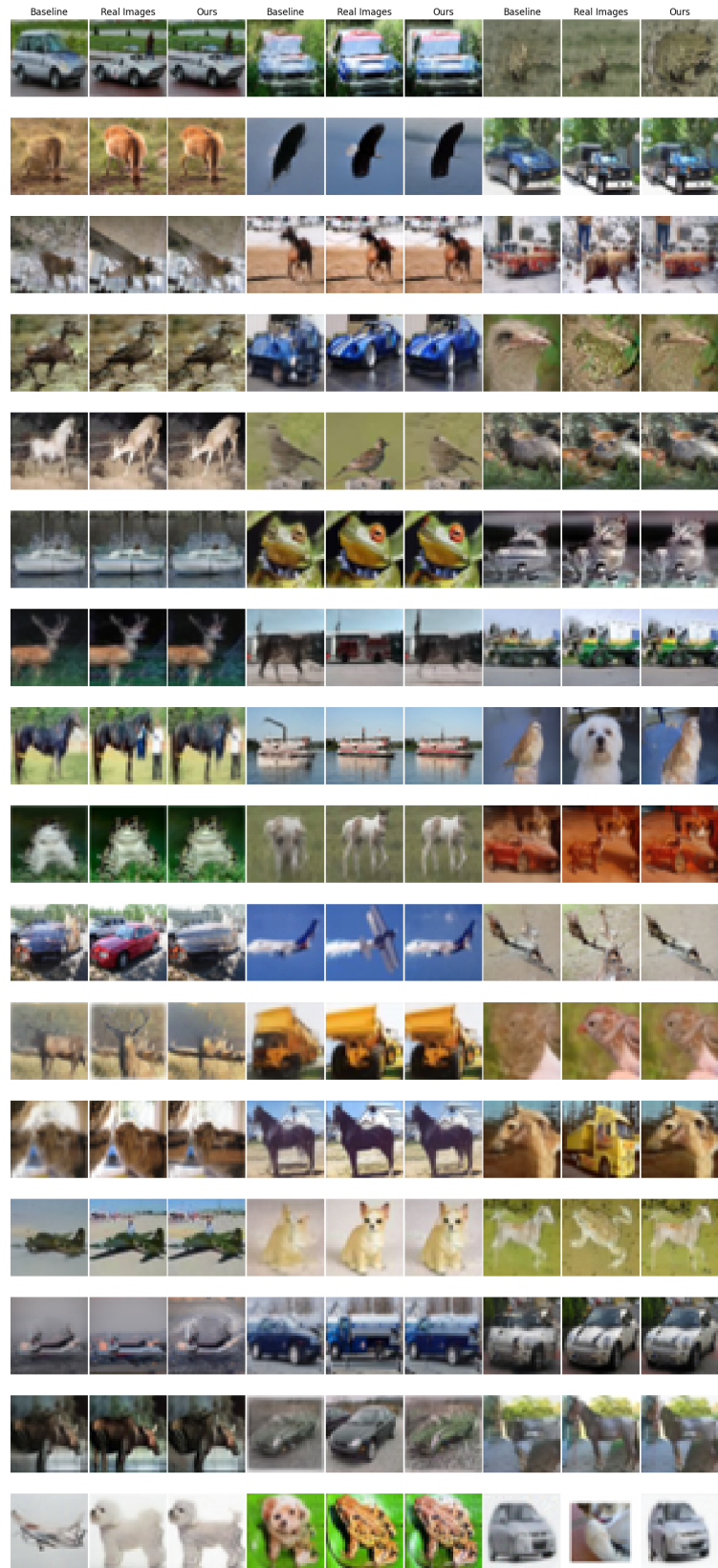


Figure A13: Compare with reconstruction image to original (1-step Euler)

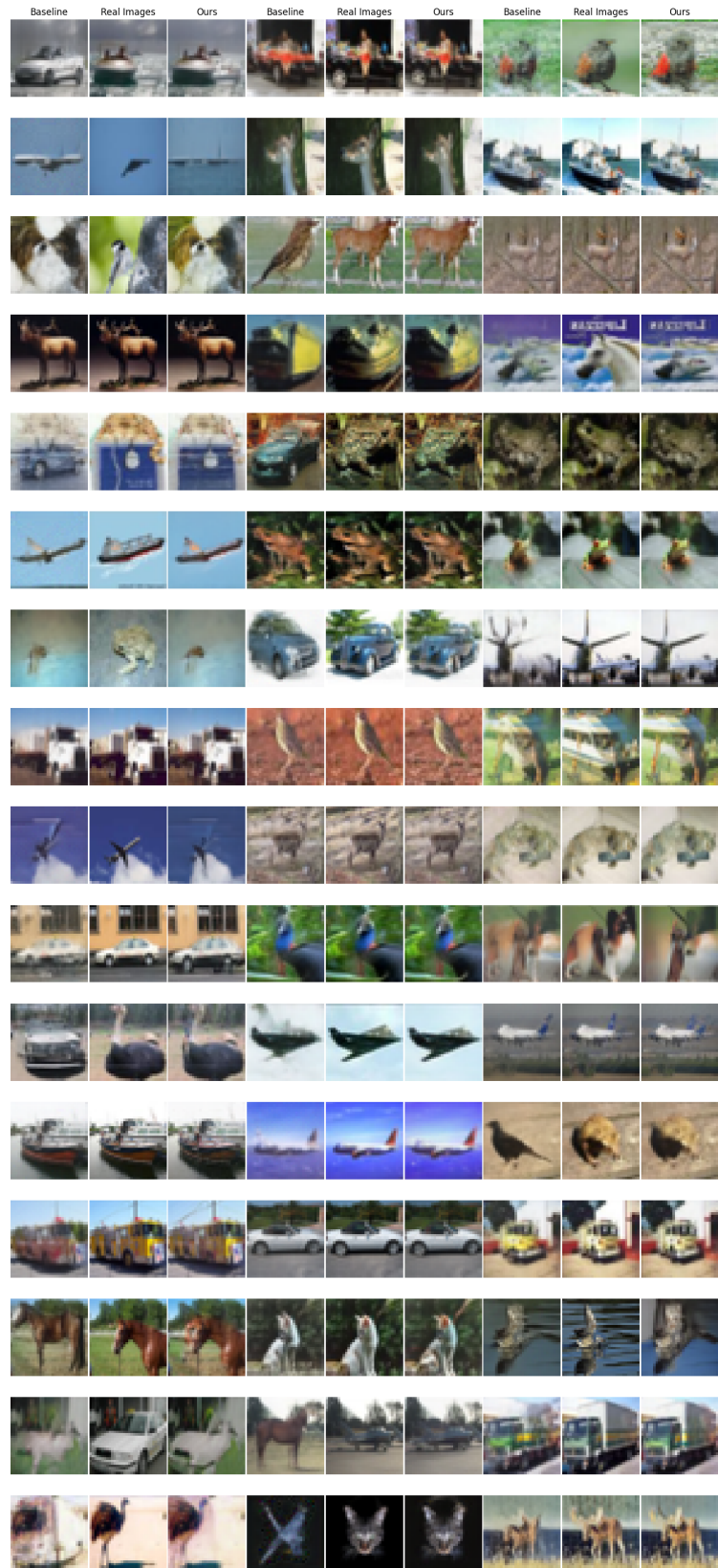


Figure A14: Compare with reconstruction image to original (1-step Euler)

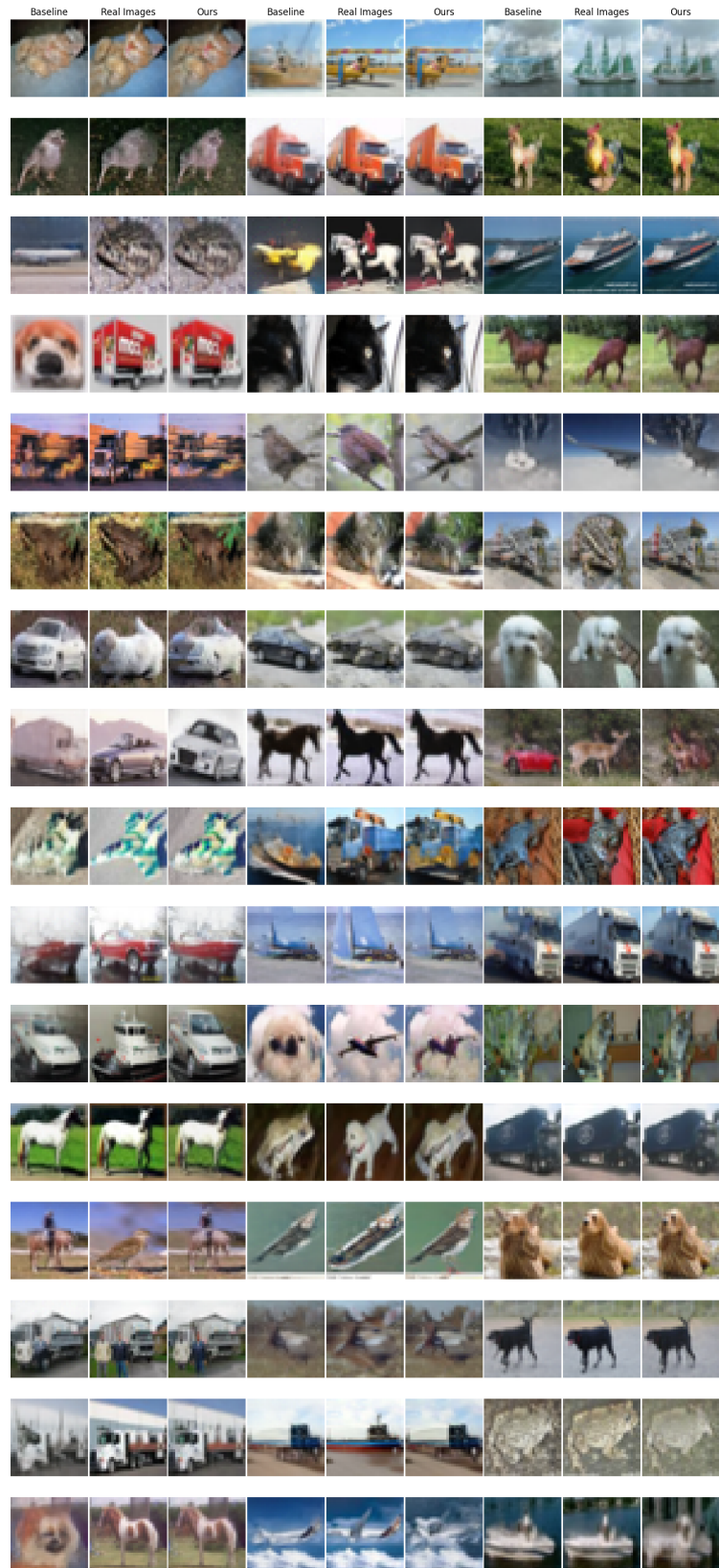


Figure A15: Compare with perturbed ( $\varepsilon = 0.04$ ) reconstruction image to original (1-step Euler)

## References

- [1] Jonas Adler, Emil Kobler, Sebastian Lunz, Carola-Bibiane Schönlieb, and Simon Arridge. Task adapted reconstruction for inverse problems. In *International Conference on Machine Learning*, pages 74–84. PMLR, 2021.
- [2] Luigi Ambrosio, Gianluca Crippa, Camillo De Lellis, Felix Otto, Michael Westdickenberg, Luigi Ambrosio, and Gianluca Crippa. Existence, uniqueness, stability and differentiability properties of the flow associated to weakly differentiable vector fields. *Transport equations and multi-D hyperbolic conservation laws*, pages 3–57, 2008.
- [3] Velin Antun, Francesco Renna, Clarice Poon, Ben Adcock, and Anders C Hansen. On instabilities of deep learning in image reconstruction and the potential costs of ai. *Proceedings of the National Academy of Sciences*, 117(48):30088–30095, 2020.
- [4] Emmanuel J Candes, Justin K Romberg, and Terence Tao. Stable signal recovery from incomplete and inaccurate measurements. *Communications on Pure and Applied Mathematics: A Journal Issued by the Courant Institute of Mathematical Sciences*, 59(8):1207–1223, 2006.
- [5] Hongrui Chen, Holden Lee, and Jianfeng Lu. Improved analysis of score-based generative modeling: User-friendly bounds under minimal smoothness assumptions. In *International Conference on Machine Learning*, pages 4735–4763. PMLR, 2023.
- [6] Valentin De Bortoli, James Thornton, Jeremy Heng, and Arnaud Doucet. Diffusion schrödinger bridge with applications to score-based generative modeling. *Advances in Neural Information Processing Systems*, 34:17695–17709, 2021.
- [7] Jia Deng, Wei Dong, Richard Socher, Li-Jia Li, Kai Li, and Li Fei-Fei. Imagenet: A large-scale hierarchical image database. In *2009 IEEE Conference on Computer Vision and Pattern Recognition (CVPR)*, pages 248–255. IEEE, 2009.
- [8] P Kingma Diederik. Adam: A method for stochastic optimization. (*No Title*), 2014.
- [9] Patrick Esser, Sumith Kulal, Andreas Blattmann, Rahim Entezari, Jonas Müller, Harry Saini, Yam Levi, Dominik Lorenz, Axel Sauer, Frederic Boesel, et al. Scaling rectified flow transformers for high-resolution image synthesis. In *Forty-first International Conference on Machine Learning*, 2024.
- [10] Alessio Figalli and Federico Glaudo. An invitation to optimal transport, wasserstein distances, and gradient flows. *Springer*, 2021.
- [11] R Flamary, N Courty, D Tuia, and A Rakotomamonjy. Optimal transport for domain adaptation. *IEEE Trans. Pattern Anal. Mach. Intell.*, 2016.
- [12] Zhengyang Geng, Ashwini Pokle, William Luo, Justin Lin, and J. Zico Kolter. Consistency models made easy, 2024. URL <https://arxiv.org/abs/2406.14548>.
- [13] Zhengyang Geng, Mingyang Deng, Xingjian Bai, J. Zico Kolter, and Kaiming He. Mean flows for one-step generative modeling, 2025. URL <https://arxiv.org/abs/2505.13447>.
- [14] Martin Heusel, Hubert Ramsauer, Thomas Unterthiner, Bernhard Nessler, and Sepp Hochreiter. Gans trained by a two time-scale update rule converge to a local nash equilibrium. *Advances in neural information processing systems*, 30, 2017.
- [15] Jonathan Ho, Ajay Jain, and Pieter Abbeel. Denoising diffusion probabilistic models. *Advances in Neural Information Processing Systems*, 33:6840–6851, 2020.
- [16] Young Kyun Jang, Dat Huynh, Ashish Shah, Wen-Kai Chen, and Ser-Nam Lim. Spherical linear interpolation and text-anchoring for zero-shot composed image retrieval. *arXiv preprint arXiv:2405.00571*, 2024.
- [17] Tero Karras, Miika Aittala, Timo Aila, and Samuli Laine. Elucidating the design space of diffusion-based generative models. *arXiv preprint arXiv:2206.00364*, 2022.
- [18] Beomsu Kim, Yu-Guan Hsieh, Michal Klein, Marco Cuturi, Jong Chul Ye, Bahjat Kawar, and James Thornton. Simple reflow: Improved techniques for fast flow models. *arXiv preprint arXiv:2410.07815*, 2024.
- [19] Dongjun Kim, Chieh-Hsin Lai, Wei-Hsiang Liao, Naoki Murata, Yuhta Takida, Toshimitsu Uesaka, Yutong He, Yuki Mitsuji, and Stefano Ermon. Consistency trajectory models: Learning probability flow ode trajectory of diffusion. *arXiv preprint arXiv:2310.02279*, 2023.

[20] Alex Krizhevsky, Geoffrey Hinton, et al. Learning multiple layers of features from tiny images. Technical report, University of Toronto, Toronto, ON, Canada, 2009. URL <https://www.cs.toronto.edu/~kriz/learning-features-2009-TR.pdf>. Technical report.

[21] Thomas G Kurtz. Equivalence of stochastic equations and martingale problems. *Stochastic analysis 2010*, pages 113–130, 2011.

[22] Tuomas Kynkänniemi, Tero Karras, Samuli Laine, Jaakko Lehtinen, and Timo Aila. Improved precision and recall metric for assessing generative models. *Advances in neural information processing systems*, 32, 2019.

[23] Sangyun Lee, Beomsu Kim, and Jong Chul Ye. Minimizing trajectory curvature of ode-based generative models. In *International Conference on Machine Learning*, pages 18957–18973. PMLR, 2023.

[24] Sangyun Lee, Zinan Lin, and Giulia Fanti. Improving the training of rectified flows. *arXiv preprint arXiv:2405.20320*, 2024.

[25] Hangyu Li, Xiangxiang Chu, Dingyuan Shi, and Lin Wang. Flowdreamer: exploring high fidelity text-to-3d generation via rectified flow, 2024. URL <https://arxiv.org/abs/2408.05008>.

[26] Yaron Lipman, Ricky T. Q. Chen, Heli Ben-Hamu, Maximilian Nickel, and Matt Le. Flow matching for generative modeling, 2023. URL <https://arxiv.org/abs/2210.02747>.

[27] Xingchao Liu, Chengyue Gong, and Qiang Liu. Flow straight and fast: Learning to generate and transfer data with rectified flow. *arXiv preprint arXiv:2209.03003*, 2022.

[28] Xingchao Liu, Xiwen Zhang, Jianzhu Ma, Jian Peng, et al. Instaflow: One step is enough for high-quality diffusion-based text-to-image generation. In *The Twelfth International Conference on Learning Representations*, 2023.

[29] Cheng Lu and Yang Song. Simplifying, stabilizing and scaling continuous-time consistency models, 2025. URL <https://arxiv.org/abs/2410.11081>.

[30] Eric Luhman and Troy Luhman. Knowledge distillation in iterative generative models for improved sampling speed. *arXiv preprint arXiv:2101.02388*, 2021.

[31] Weijian Luo, Tianyang Hu, Shifeng Zhang, Jiacheng Sun, Zhenguo Li, and Zhihua Zhang. Diff-instruct: A universal approach for transferring knowledge from pre-trained diffusion models. *Advances in Neural Information Processing Systems*, 36, 2024.

[32] Fabian Pedregosa, Gael Varoquaux, Alexandre Gramfort, Vincent Michel, Bertrand Thirion, Olivier Grisel, Mathieu Blondel, Peter Prettenhofer, Ron Weiss, Vincent Dubourg, Jake Vanderplas, Alexandre Passos, David Cournapeau, Matthieu Brucher, Matthieu Perrot, and É.douard Duchesnay. Scikit-learn: Machine learning in python. *Journal of Machine Learning Research*, 12:2825–2830, 2011.

[33] Saiprasad Ravishankar, Jong Chul Ye, and Jeffrey A Fessler. Image reconstruction: From sparsity to data-adaptive methods and machine learning. *Proceedings of the IEEE*, 108(1):86–109, 2019.

[34] Tim Salimans and Jonathan Ho. Progressive distillation for fast sampling of diffusion models. *arXiv preprint arXiv:2202.00512*, 2022.

[35] Jiaming Song, Chenlin Meng, and Stefano Ermon. Denoising diffusion implicit models. *arXiv preprint arXiv:2010.02502*, 2020.

[36] Yang Song and Prafulla Dhariwal. Improved techniques for training consistency models. *arXiv preprint arXiv:2310.14189*, 2023.

[37] Yang Song, Jascha Sohl-Dickstein, Diederik P Kingma, Abhishek Kumar, Stefano Ermon, and Ben Poole. Score-based generative modeling through stochastic differential equations. *arXiv preprint arXiv:2011.13456*, 2020.

[38] Yang Song, Prafulla Dhariwal, Mark Chen, and Ilya Sutskever. Consistency models. *arXiv preprint arXiv:2303.01469*, 2023.

[39] Hans J Stetter et al. *Analysis of discretization methods for ordinary differential equations*, volume 23. Springer, 1973.

[40] Alexander Tong, Kilian Fatras, Nikolay Malkin, Guillaume Huguet, Yanlei Zhang, Jarrid Rector-Brooks, Guy Wolf, and Yoshua Bengio. Improving and generalizing flow-based generative models with minibatch optimal transport, 2024. URL <https://arxiv.org/abs/2302.00482>.

[41] Belinda Tzen and Maxim Raginsky. Theoretical guarantees for sampling and inference in generative models with latent diffusions. In *Conference on Learning Theory*, pages 3084–3114. PMLR, 2019.

[42] Arash Vahdat, Karsten Kreis, and Jan Kautz. Score-based generative modeling in latent space. *Advances in Neural Information Processing Systems*, 34:11287–11302, 2021.

[43] Francisco Vargas, Pierre Thodoroff, Austen Lamacraft, and Neil Lawrence. Solving schrödinger bridges via maximum likelihood. *Entropy*, 23(9):1134, 2021.

[44] Cedric Villani. Optimal transport: old and new. *Springer*, 2009.

[45] Cedric Villani. Topics in optimal transportation. *American Mathematical Soc*, 2021.

[46] Pauli Virtanen, Ralf Gommers, Travis E Oliphant, Matt Haberland, Tyler Reddy, David Cournapeau, Evgeni Burovski, Pearu Peterson, Warren Weckesser, Jonathan Bright, et al. Scipy 1.0: fundamental algorithms for scientific computing in python. *Nature methods*, 17(3):261–272, 2020.

[47] Clinton Wang and Polina Golland. Interpolating between images with diffusion models, 2023. URL <https://openreview.net/pdf?id=L2D9Gybx0P>. OpenReview preprint.

[48] Fu-Yun Wang, Ling Yang, Zhaoyang Huang, Mengdi Wang, and Hongsheng Li. Rectified diffusion: Straightness is not your need in rectified flow. *arXiv preprint arXiv:2410.07303*, 2024.

[49] Yilun Xu, Ziming Liu, Max Tegmark, and Tommi Jaakkola. Poisson flow generative models. *Advances in Neural Information Processing Systems*, 35:16782–16795, 2022.

[50] Hanshu Yan, Xingchao Liu, Jiachun Pan, Jun Hao Liew, Qiang Liu, and Jiashi Feng. Perflow: Piecewise rectified flow as universal plug-and-play accelerator, 2024. URL <https://arxiv.org/abs/2405.07510>.

[51] Tianwei Yin, Michaël Gharbi, Richard Zhang, Eli Shechtman, Fredo Durand, William T Freeman, and Taesung Park. One-step diffusion with distribution matching distillation. In *Proceedings of the IEEE/CVF Conference on Computer Vision and Pattern Recognition*, pages 6613–6623, 2024.

[52] Fisher Yu, Ari Seff, Yinda Zhang, Shuran Song, Thomas Funkhouser, and Jianxiong Xiao. Lsun: Construction of a large-scale image dataset using deep learning with humans in the loop. *arXiv preprint arXiv:1506.03365*, 2015.

[53] Hongkai Zheng, Weili Nie, Arash Vahdat, Kamyar Azizzadenesheli, and Anima Anandkumar. Fast sampling of diffusion models via operator learning. In *International conference on machine learning*, pages 42390–42402. PMLR, 2023.

[54] Linqi Zhou, Stefano Ermon, and Jiaming Song. Inductive moment matching, 2025. URL <https://arxiv.org/abs/2503.07565>.

[55] Mingyuan Zhou, Huangjie Zheng, Zhendong Wang, Mingzhang Yin, and Hai Huang. Score identity distillation: Exponentially fast distillation of pretrained diffusion models for one-step generation. In *Forty-first International Conference on Machine Learning*, 2024.

[56] Huminhao Zhu, Fangyikang Wang, Tianyu Ding, Qing Qu, and Zhihui Zhu. Analyzing and improving model collapse in rectified flow models. *arXiv preprint arXiv:2412.08175*, 2024.

[57] Yuanzhi Zhu, Xingchao Liu, and Qiang Liu. Slimflow: Training smaller one-step diffusion models with rectified flow, 2024. URL <https://arxiv.org/abs/2407.12718>.

## Additional References

[A1] Stanczuk, Jan Paweł, Georgios Batzolis, Teo Deveney, and Carola-Bibiane Schönlieb. *Diffusion models encode the intrinsic dimension of data manifolds*. International Conference on Machine Learning (ICML), 2024.

[A2] Mingi Kwon, Shin seong Kim, Jaeseok Jeong, Yi Ting Hsiao, and Youngjung Uh. Tcfg: *Tangential damping classifier-free guidance*. 2025. URL <https://arxiv.org/abs/2503.18137>.

[A3] Dhariwal, Prafulla and Alexander Nichol. *Diffusion models beat GANs on image synthesis*. Advances in Neural Information Processing Systems (NeurIPS), 34:8780–8794, 2021.

## NeurIPS Paper Checklist

### 1. Claims

Question: Do the main claims made in the abstract and introduction accurately reflect the paper's contributions and scope?

Answer: [\[Yes\]](#)

Justification: We have summarized our contributions at the end of the introduction.

Guidelines:

- The answer NA means that the abstract and introduction do not include the claims made in the paper.
- The abstract and/or introduction should clearly state the claims made, including the contributions made in the paper and important assumptions and limitations. A No or NA answer to this question will not be perceived well by the reviewers.
- The claims made should match theoretical and experimental results, and reflect how much the results can be expected to generalize to other settings.
- It is fine to include aspirational goals as motivation as long as it is clear that these goals are not attained by the paper.

### 2. Limitations

Question: Does the paper discuss the limitations of the work performed by the authors?

Answer: [\[Yes\]](#)

Justification: See Appendix L.

Guidelines:

- The answer NA means that the paper has no limitation while the answer No means that the paper has limitations, but those are not discussed in the paper.
- The authors are encouraged to create a separate "Limitations" section in their paper.
- The paper should point out any strong assumptions and how robust the results are to violations of these assumptions (e.g., independence assumptions, noiseless settings, model well-specification, asymptotic approximations only holding locally). The authors should reflect on how these assumptions might be violated in practice and what the implications would be.
- The authors should reflect on the scope of the claims made, e.g., if the approach was only tested on a few datasets or with a few runs. In general, empirical results often depend on implicit assumptions, which should be articulated.
- The authors should reflect on the factors that influence the performance of the approach. For example, a facial recognition algorithm may perform poorly when image resolution is low or images are taken in low lighting. Or a speech-to-text system might not be used reliably to provide closed captions for online lectures because it fails to handle technical jargon.
- The authors should discuss the computational efficiency of the proposed algorithms and how they scale with dataset size.
- If applicable, the authors should discuss possible limitations of their approach to address problems of privacy and fairness.
- While the authors might fear that complete honesty about limitations might be used by reviewers as grounds for rejection, a worse outcome might be that reviewers discover limitations that aren't acknowledged in the paper. The authors should use their best judgment and recognize that individual actions in favor of transparency play an important role in developing norms that preserve the integrity of the community. Reviewers will be specifically instructed to not penalize honesty concerning limitations.

### 3. Theory assumptions and proofs

Question: For each theoretical result, does the paper provide the full set of assumptions and a complete (and correct) proof?

Answer: [\[NA\]](#)

Justification: The paper does not present formal theoretical results or proofs. Instead, we focus on empirically analyzing and mitigating distributional drift during the reflow process.

Guidelines:

- The answer NA means that the paper does not include theoretical results.
- All the theorems, formulas, and proofs in the paper should be numbered and cross-referenced.
- All assumptions should be clearly stated or referenced in the statement of any theorems.

- The proofs can either appear in the main paper or the supplemental material, but if they appear in the supplemental material, the authors are encouraged to provide a short proof sketch to provide intuition.
- Inversely, any informal proof provided in the core of the paper should be complemented by formal proofs provided in appendix or supplemental material.
- Theorems and Lemmas that the proof relies upon should be properly referenced.

#### 4. Experimental result reproducibility

Question: Does the paper fully disclose all the information needed to reproduce the main experimental results of the paper to the extent that it affects the main claims and/or conclusions of the paper (regardless of whether the code and data are provided or not)?

Answer: [\[Yes\]](#)

Justification: We describe the full training mechanism of our method, including hyperparameter settings, in the Section 3.5 and Appendix A. Additionally, we provide the pseudo algorithm and detailed training configurations for each dataset in the Appendix K.

Guidelines:

- The answer NA means that the paper does not include experiments.
- If the paper includes experiments, a No answer to this question will not be perceived well by the reviewers: Making the paper reproducible is important, regardless of whether the code and data are provided or not.
- If the contribution is a dataset and/or model, the authors should describe the steps taken to make their results reproducible or verifiable.
- Depending on the contribution, reproducibility can be accomplished in various ways. For example, if the contribution is a novel architecture, describing the architecture fully might suffice, or if the contribution is a specific model and empirical evaluation, it may be necessary to either make it possible for others to replicate the model with the same dataset, or provide access to the model. In general, releasing code and data is often one good way to accomplish this, but reproducibility can also be provided via detailed instructions for how to replicate the results, access to a hosted model (e.g., in the case of a large language model), releasing of a model checkpoint, or other means that are appropriate to the research performed.
- While NeurIPS does not require releasing code, the conference does require all submissions to provide some reasonable avenue for reproducibility, which may depend on the nature of the contribution. For example
  - (a) If the contribution is primarily a new algorithm, the paper should make it clear how to reproduce that algorithm.
  - (b) If the contribution is primarily a new model architecture, the paper should describe the architecture clearly and fully.
  - (c) If the contribution is a new model (e.g., a large language model), then there should either be a way to access this model for reproducing the results or a way to reproduce the model (e.g., with an open-source dataset or instructions for how to construct the dataset).
  - (d) We recognize that reproducibility may be tricky in some cases, in which case authors are welcome to describe the particular way they provide for reproducibility. In the case of closed-source models, it may be that access to the model is limited in some way (e.g., to registered users), but it should be possible for other researchers to have some path to reproducing or verifying the results.

#### 5. Open access to data and code

Question: Does the paper provide open access to the data and code, with sufficient instructions to faithfully reproduce the main experimental results, as described in supplemental material?

Answer: [\[Yes\]](#)

Justification: We provide a partial implementation with core components in Appendix M, and plan to release the full codebase and instructions by the camera-ready deadline.

Guidelines:

- The answer NA means that paper does not include experiments requiring code.
- Please see the NeurIPS code and data submission guidelines (<https://nips.cc/public/guides/CodeSubmissionPolicy>) for more details.
- While we encourage the release of code and data, we understand that this might not be possible, so “No” is an acceptable answer. Papers cannot be rejected simply for not including code, unless this is central to the contribution (e.g., for a new open-source benchmark).

- The instructions should contain the exact command and environment needed to run to reproduce the results. See the NeurIPS code and data submission guidelines (<https://nips.cc/public/guides/CodeSubmissionPolicy>) for more details.
- The authors should provide instructions on data access and preparation, including how to access the raw data, preprocessed data, intermediate data, and generated data, etc.
- The authors should provide scripts to reproduce all experimental results for the new proposed method and baselines. If only a subset of experiments are reproducible, they should state which ones are omitted from the script and why.
- At submission time, to preserve anonymity, the authors should release anonymized versions (if applicable).
- Providing as much information as possible in supplemental material (appended to the paper) is recommended, but including URLs to data and code is permitted.

## 6. Experimental setting/details

Question: Does the paper specify all the training and test details (e.g., data splits, hyperparameters, how they were chosen, type of optimizer, etc.) necessary to understand the results?

Answer: [\[Yes\]](#)

Justification: We provide clear guidelines for choosing the perturbation magnitude in the Section 3.5, and describe all model configurations including the optimizer in both the Experiment Setup Section 4 and the Appendix J.

Guidelines:

- The answer NA means that the paper does not include experiments.
- The experimental setting should be presented in the core of the paper to a level of detail that is necessary to appreciate the results and make sense of them.
- The full details can be provided either with the code, in appendix, or as supplemental material.

## 7. Experiment statistical significance

Question: Does the paper report error bars suitably and correctly defined or other appropriate information about the statistical significance of the experiments?

Answer: [\[Yes\]](#)

Justification: We explicitly state the number of data points used to compute the mean values of curvature, initial velocity delta, and reconstruction error in Section 4 and Appendix J. The magnitude of the epsilon used to calculate the perturbed reconstruction error is also clearly described. Additionally, we specify the number of synthetic samples used for evaluating generation quality metrics such as recall, precision, and FID.

Guidelines:

- The answer NA means that the paper does not include experiments.
- The authors should answer "Yes" if the results are accompanied by error bars, confidence intervals, or statistical significance tests, at least for the experiments that support the main claims of the paper.
- The factors of variability that the error bars are capturing should be clearly stated (for example, train/test split, initialization, random drawing of some parameter, or overall run with given experimental conditions).
- The method for calculating the error bars should be explained (closed form formula, call to a library function, bootstrap, etc.)
- The assumptions made should be given (e.g., Normally distributed errors).
- It should be clear whether the error bar is the standard deviation or the standard error of the mean.
- It is OK to report 1-sigma error bars, but one should state it. The authors should preferably report a 2-sigma error bar than state that they have a 96% CI, if the hypothesis of Normality of errors is not verified.
- For asymmetric distributions, the authors should be careful not to show in tables or figures symmetric error bars that would yield results that are out of range (e.g. negative error rates).
- If error bars are reported in tables or plots, The authors should explain in the text how they were calculated and reference the corresponding figures or tables in the text.

## 8. Experiments compute resources

Question: For each experiment, does the paper provide sufficient information on the computer resources (type of compute workers, memory, time of execution) needed to reproduce the experiments?

Answer: [\[Yes\]](#)

Justification: We provide the details of our CPU and GPU resources in the appendix A. Additionally, the number of training iterations, batch size, and the number of fake and real samples used in each experiment are specified in the experiment section 4 and Appendix J.

Guidelines:

- The answer NA means that the paper does not include experiments.
- The paper should indicate the type of compute workers CPU or GPU, internal cluster, or cloud provider, including relevant memory and storage.
- The paper should provide the amount of compute required for each of the individual experimental runs as well as estimate the total compute.
- The paper should disclose whether the full research project required more compute than the experiments reported in the paper (e.g., preliminary or failed experiments that didn't make it into the paper).

## 9. Code of ethics

Question: Does the research conducted in the paper conform, in every respect, with the NeurIPS Code of Ethics <https://neurips.cc/public/EthicsGuidelines>?

Answer: [\[Yes\]](#)

Justification: We confirm that the research conducted in this paper adheres to the NeurIPS Code of Ethics.

Guidelines:

- The answer NA means that the authors have not reviewed the NeurIPS Code of Ethics.
- If the authors answer No, they should explain the special circumstances that require a deviation from the Code of Ethics.
- The authors should make sure to preserve anonymity (e.g., if there is a special consideration due to laws or regulations in their jurisdiction).

## 10. Broader impacts

Question: Does the paper discuss both potential positive societal impacts and negative societal impacts of the work performed?

Answer: [\[No\]](#)

Justification: This work analyzes distributional drift in reflow and proposes a technical solution for flow-based generative models. Since it does not involve application-specific deployment or sensitive content, we found no broader societal impacts to discuss.

Guidelines:

- The answer NA means that there is no societal impact of the work performed.
- If the authors answer NA or No, they should explain why their work has no societal impact or why the paper does not address societal impact.
- Examples of negative societal impacts include potential malicious or unintended uses (e.g., disinformation, generating fake profiles, surveillance), fairness considerations (e.g., deployment of technologies that could make decisions that unfairly impact specific groups), privacy considerations, and security considerations.
- The conference expects that many papers will be foundational research and not tied to particular applications, let alone deployments. However, if there is a direct path to any negative applications, the authors should point it out. For example, it is legitimate to point out that an improvement in the quality of generative models could be used to generate deepfakes for disinformation. On the other hand, it is not needed to point out that a generic algorithm for optimizing neural networks could enable people to train models that generate Deepfakes faster.
- The authors should consider possible harms that could arise when the technology is being used as intended and functioning correctly, harms that could arise when the technology is being used as intended but gives incorrect results, and harms following from (intentional or unintentional) misuse of the technology.
- If there are negative societal impacts, the authors could also discuss possible mitigation strategies (e.g., gated release of models, providing defenses in addition to attacks, mechanisms for monitoring misuse, mechanisms to monitor how a system learns from feedback over time, improving the efficiency and accessibility of ML).

## 11. Safeguards

Question: Does the paper describe safeguards that have been put in place for responsible release of data or models that have a high risk for misuse (e.g., pretrained language models, image generators, or scraped datasets)?

Answer: [NA]

Justification: : This work does not involve any models or datasets that pose a foreseeable risk of misuse or harm.

Guidelines:

- The answer NA means that the paper poses no such risks.
- Released models that have a high risk for misuse or dual-use should be released with necessary safeguards to allow for controlled use of the model, for example by requiring that users adhere to usage guidelines or restrictions to access the model or implementing safety filters.
- Datasets that have been scraped from the Internet could pose safety risks. The authors should describe how they avoided releasing unsafe images.
- We recognize that providing effective safeguards is challenging, and many papers do not require this, but we encourage authors to take this into account and make a best faith effort.

## 12. Licenses for existing assets

Question: Are the creators or original owners of assets (e.g., code, data, models), used in the paper, properly credited and are the license and terms of use explicitly mentioned and properly respected?

Answer: [Yes]

Justification: We used the official repositories of existing flow models [27] and clearly cited the datasets used for training (CIFAR-10 [20], LSUN [52], ImageNet [7]). We also specified the version of the Runge-Kutta sampling tool (from SciPy ) used during sampling [46].

Guidelines:

- The answer NA means that the paper does not use existing assets.
- The authors should cite the original paper that produced the code package or dataset.
- The authors should state which version of the asset is used and, if possible, include a URL.
- The name of the license (e.g., CC-BY 4.0) should be included for each asset.
- For scraped data from a particular source (e.g., website), the copyright and terms of service of that source should be provided.
- If assets are released, the license, copyright information, and terms of use in the package should be provided. For popular datasets, [paperswithcode.com/datasets](http://paperswithcode.com/datasets) has curated licenses for some datasets. Their licensing guide can help determine the license of a dataset.
- For existing datasets that are re-packaged, both the original license and the license of the derived asset (if it has changed) should be provided.
- If this information is not available online, the authors are encouraged to reach out to the asset's creators.

## 13. New assets

Question: Are new assets introduced in the paper well documented and is the documentation provided alongside the assets?

Answer: [NA]

Justification: We do not introduce any new assets. All experiments are conducted using widely used public datasets such as CIFAR-10, ImageNet, and LSUN Bedroom [20, 52, 7].

Guidelines:

- The answer NA means that the paper does not release new assets.
- Researchers should communicate the details of the dataset/code/model as part of their submissions via structured templates. This includes details about training, license, limitations, etc.
- The paper should discuss whether and how consent was obtained from people whose asset is used.
- At submission time, remember to anonymize your assets (if applicable). You can either create an anonymized URL or include an anonymized zip file.

## 14. Crowdsourcing and research with human subjects

Question: For crowdsourcing experiments and research with human subjects, does the paper include the full text of instructions given to participants and screenshots, if applicable, as well as details about compensation (if any)?

Answer: [NA]

Justification: This paper does not involve crowdsourcing or research with human subjects.

Guidelines:

- The answer NA means that the paper does not involve crowdsourcing nor research with human subjects.
- Including this information in the supplemental material is fine, but if the main contribution of the paper involves human subjects, then as much detail as possible should be included in the main paper.
- According to the NeurIPS Code of Ethics, workers involved in data collection, curation, or other labor should be paid at least the minimum wage in the country of the data collector.

#### 15. Institutional review board (IRB) approvals or equivalent for research with human subjects

Question: Does the paper describe potential risks incurred by study participants, whether such risks were disclosed to the subjects, and whether Institutional Review Board (IRB) approvals (or an equivalent approval/review based on the requirements of your country or institution) were obtained?

Answer: [NA]

Justification: This paper does not involve crowdsourcing nor research with human subjects.

Guidelines:

- The answer NA means that the paper does not involve crowdsourcing nor research with human subjects.
- Depending on the country in which research is conducted, IRB approval (or equivalent) may be required for any human subjects research. If you obtained IRB approval, you should clearly state this in the paper.
- We recognize that the procedures for this may vary significantly between institutions and locations, and we expect authors to adhere to the NeurIPS Code of Ethics and the guidelines for their institution.
- For initial submissions, do not include any information that would break anonymity (if applicable), such as the institution conducting the review.

#### 16. Declaration of LLM usage

Question: Does the paper describe the usage of LLMs if it is an important, original, or non-standard component of the core methods in this research? Note that if the LLM is used only for writing, editing, or formatting purposes and does not impact the core methodology, scientific rigorosity, or originality of the research, declaration is not required.

Answer: [NA]

Justification: We did not use LLMs for any part of the core methodology or scientific contribution of the paper.

Guidelines:

- The answer NA means that the core method development in this research does not involve LLMs as any important, original, or non-standard components.
- Please refer to our LLM policy (<https://neurips.cc/Conferences/2025/LLM>) for what should or should not be described.